Lithos 202–203 (2014) 100–119

Contents lists available at ScienceDirect

Lithos

journal homepage: www.elsevier.com/locate/lithos

The Gifford Creek Ferrocarbonatite Complex, Gascoyne Province, Western Australia: Associated fenitic alteration and a putative link with the ~1075 Ma Warakurna LIP

Franco Pirajno [a,b,*], Ignacio González-Álvarez [b,c], Wei Chen [d], Kurt T. Kyser [e], Antonio Simonetti [d], Evelyne Leduc [e], Monica leGras [c]

[a] Geological Survey of Western Australia, Mineral House, 100 Plain Street, East Perth, WA 6004, Australia
[b] Centre for Exploration Targeting, University of Western Australia, 35 Stirling Hwy, Crawley, WA 6009, Australia
[c] CSIRO, Earth Science and Resource Engineering, 26 Dick Perry Av., Discovery Theme, Minerals Down Under Flagship, Kensington 6151, Australia
[d] Department of Civil Engineering and Geological Sciences, 156 Fitzpatrick Hall, University of Notre Dame, Notre Dame, IN 46556, USA
[e] Department of Geological Sciences and Geological Engineering, Queens University, Kingston, Ontario K7 3N6, Canada

ARTICLE INFO

Article history:
Received 13 December 2013
Accepted 13 May 2014
Available online 27 May 2014

Keywords:
Carbonatite
Fenitic alteration
Apatite and monazite dating
Warakurna LIP
Mantle plume
Gifford Creek, Gascoyne Province

ABSTRACT

The Gifford Creek Ferrocarbonatite Complex (GFC), located in the Neoarchean–Palaeoproterozoic Gascoyne Province, Western Australia, comprises sills, dykes, and veins of ferrocarbonatite intruding the Pimbyana Granite and Yangibana Granite of the Durlacher Supersuite and metasedimentary rocks of the Pooranoo Metamorphics. The ferrocarbonatites are associated with complex and irregularly distributed zones of fenitic alteration. These ferrocarbonatites and fenites are also associated with a swarm of ironstone veins, containing magnetite, hematite and goethite. The GFC and associated fenite outcrops are distributed within a ~700 km^2 area, north of the Lyons River Fault. Ferrocarbonatite sills and dykes are predominant in a northwest-trending belt, along the southern margin of the complex; whereas ferrocarbonatite veins tend to be distributed in a series of sub-parallel west–northwest-trending linear belts, generally associated with the Fe oxide veins with sinuous trends. These veins have margins of Fe-rich carbonates associated with zones of alteration that have a fenitic character. The fenitic haloes are characterised by the presence of Na–K-feldspars and/or Na-amphiboles and magnetite. In some cases monomineralic feldspar zones (orthoclasite) are present. Fenitic alteration is spatially associated with the carbonatites, but it can also form discrete veins and veinlets in basement granitic rocks (Pimbyana and Yangibana Granites). Petrographic, XRD and SEM analyses show that the ferrocarbonatites are dominantly composed of ankerite–dolomite, magnetite, arfvedsonite–riebeckite, and lesser calcite. Alkali amphibole has compositions ranging from potassian magnesio-arfvedsonite to magnesio-riebeckite. Sills and dykes north of the Lyons River, are characterised by a carbonate-rich matrix, containing >50 vol.% ankerite–dolomite, with accessory quantities of apatite, barite, monazite, and phlogopite. In-situ U–Pb age determination of apatite grains by LA-ICP-MS on a sample of ferrocarbonatite was performed and an average age of 1075 ± 35 Ma was obtained. This age is within the range of ages (~1078–1070 Ma) of the Warakurna Large Igneous Province (WLIP) and we suggest that the GFC is related to the mantle plume event that generated the WLIP. This is a significant outcome, because it may lead to the recognition or discovery of other carbonatites within the area covered by the WLIP. In addition, monazite from fenitic rocks associated with the ironstones yielded an age of 1050 ± 25 Ma, suggesting that a second phase of carbonatite magmatism occurred, resulting in the emplacement of the carbonatite-ironstone veins swarm. A model is proposed to explain the formation of the GFC system.

1. Introduction

During the last decade or so, carbonatites and alkaline igneous complexes have gained greater economic importance, due to the high demand of rare earth elements (REE), in their wide applications for wind turbines, catalysts, TVs, computer screens, hybrid batteries, video cameras, etc. (Chakhmouradian and Wall, 2012). Apart from REE, other elements of economic value in carbonatites and alkaline complexes include: Cu, Fe, P, F, Ba, Nb, U, Sr, Au, Pb and Zn (e.g., Hoatson et al., 2011). Styles of mineralisation are principally disseminations, late-stage replacement bodies and hydrothermal veins and lenses. Carbonatites, together with alkali igneous complexes, are part of intraplate anorogenic magmatism.

* Corresponding author at: Geological Survey of Western Australia, Mineral House, 100 Plain Street, East Perth, WA 6004, Australia. Tel.: +61 892223155; fax: +61 892223633.
E-mail address: franco.pirajno@uwa.edu.au (F. Pirajno).

http://dx.doi.org/10.1016/j.lithos.2014.05.012
0024-4937/

Typical lithological associations of alkaline magmatism include: kimberlites, mafic ultrapotassic rocks, syenite–pyroxenite–ijolite–carbonatite assemblages, carbonatite, alkali basalts and peralkaline granite–syenite–gabbro assemblages (Mutschler et al., 1985).

Kimberlites, lamproites and carbonatites are known to have isotopic signatures (He, Os, Sr, Nd, Pb and O) similar to ocean island basalts, and as such are considered as part of mantle plume magmatism (Bell, 2001; Ernst and Bell, 2010), although cases have also been cited for a non-mantle plume origin (e.g. Lentz, 1999) or to a subduction system (D'Orazio et al., 2007). In general though, it is contended that carbonatites may represent distal expressions resulting from the channelling of plume material along pre-existing lithospheric breaks, with small degrees of melting of enriched/metasomatised lithosphere and/or crustal melts. Begg et al. (2009, 2010) and Ebinger and Sleep (1998) suggested that a mantle plume might focus its flow towards craton–mobile belt boundaries, where at depths of >150 km small volumes of melt can be produced by decompression. Kimberlite and lamproites are well known for their diamondiferous potential, whereas carbonatite may host important resources of rare metals, REE and Cu (Hoatson et al., 2011; Pirajno, 2000).

The origin of carbonatite magma remains controversial (Downes et al., 2012), and central to this controversy is the relationship between carbonatites and the silica-undersaturated rocks with which they are commonly associated. Three main theories have been proposed to explain the origin of carbonatite: 1) as the result of evolving via fractional crystallisation at crustal pressures of a mantle-derived carbonate-rich alkali silicate melt (e.g., Bell et al., 1999; Watkinson and Wyllie, 1971); 2) as the direct result of melting of dolomite–peridotite within the mantle (e.g. Eggler, 1989; Gittins, 1989); and 3) as immiscible separation of a carbonatite liquid from an originally homogeneous carbonated silicate melt, the stage of separation determining the composition of both conjugate magmas (e.g., Kjarsgaard and Hamilton, 1989; Le Bas, 1987, 1989; Mitchell, 2005).

Some of the important carbonatite-associated mineral deposits include the Phalaborwa complex, Glenover, Kruidfontein, Pilanesberg, and Schiel (all in South Africa), Dorowa, Shawa and Gunga (Zimbabwe), Okorusu, Kalkfeld and Ondurakorume (Namibia), the giant Bayan Obo (China), Mountain Pass (California, USA), Araxa (Brazil) and Mount Weld (Western Australia). Woolley and Kjarsgaard (2008) provided a world-wide catalogue of carbonatites, listing a total of 527 known occurrences, including the Gifford Creek Ferrocarbonatite Complex (henceforth referred to as GFC), which constitutes the topic of this contribution.

In this study, we report the results of our work on the ferrocarbonatites and the associated ironstone veins that constitute the GFC, Gascoyne Province, Western Australia. Our study was carried out on the basis of field observations and the integration of petrography (by conventional optical microscopy, Scanning Electron Microscopy, SEM; and X-ray Diffraction, XRD), and whole-rock geochemistry. Based on the above, we developed a model that attempts to explain the origin of the ferrocarbonatite–ironstone association. Furthermore, we report age data obtained from primary apatites contained in ferrocarbonatite and from monazites contained in fenitic rocks associated with the ironstone veins. The apatites yielded an age of ~1075 Ma, whereas the monazites returned an age of ~1050 Ma, suggesting two distinct events. The former fits, within error, with the age of Warakurna Large Igneous Province (WLIP; Wingate et al., 2004), which covers an area of at least 1.5×10^6 km^2, extending from western–central Australia across the Capricorn Orogen and the Gascoyne Province (Pirajno and Hoatson, 2012). This makes the GFC the first recorded carbonatite system associated with the WLIP.

2. Geological setting

The GFC lies within the Gascoyne Province of the Capricorn Orogen, located between the Archean Yilgarn and Pilbara cratons, and overlain by the Palaeoproterozoic Ashburton Basin to the north, the Mesoproterozoic Edmund and Collier Basins to the east and the Phanerozoic Carnarvon Basin to the west (Fig. 1). The Gascoyne Province consists of a suite of Neoarchean to Palaeoproterozoic granite gneisses and metasedimentary rocks (Johnson et al., 2011a,b) that are interpreted as basement to various Proterozoic rocks, including granitic rocks of the 1680–1620 Ma Durlacher Supersuite and the metasedimentary rocks of the 1760–1680 Ma Pooranoo Metamorphics. Details of the geology of the province are provided by Johnson et al. (2011a), Martin et al. (2006), and Sheppard et al. (2007, 2010), and an overview of its mineralization by Flint and Abeysinghe (2000). In the Gascoyne Province, at least six tectono-thermal events have been recognised: 1) 2005–1950 Ma Glenburgh Orogeny (Johnson et al., 2011b,c); 2) 1820–1770 Ma Capricorn Orogeny (Sheppard et al., 2011); 3) 1680–1620 Ma Mangaroon Orogeny (Sheppard et al., 2007); 4) 1385–1170 Ma Mutherbukin Tectonic Event (Johnson et al., 2009, 2011c); 5) 1030–955 Ma Edmundian Orogeny (Sheppard et al., 2007), and 6) a possible Neoproterozoic event at ~570 Ma, the Mulka Tectonic Event (Sheppard et al., 2010). The Gascoyne Province was later intruded by the 755 Ma Mundine Well Dolerite Suite (Wingate and Giddings, 2000), and then cut by east–southeast-trending shear zones at 570 Ma (Mulka event; Sheppard et al., 2010).

Pearson (1996), Pearson and Taylor (1996) and Pearson et al. (1996), first studied altered rocks, dykes of alkaline composition and associated ironstone veins, intruding the Proterozoic granitic rocks of the Gascoyne Province. Two alkaline magmatic episodes were described: (1) a swarm of ultrabasic intrusions emplaced prior to the deposition of the Bangemall Supergroup at ~1680, and (2) a younger phase of dykes and sills of carbonatitic affinity that intrude the Bangemall Supergroup. They named these alkaline rocks, the Gifford Creek Igneous Complex.

On the basis of Pearson and co-authors' work and our own studies, we confirm the Gifford Creek Complex to be a carbonatite complex (rocks with >50% carbonates, fluoroapatite, nepheline and other feldspathoids), comprising ferrocarbonatite dykes, veins and sills that are surrounded by variably fenitised country rocks. Hence, it was first renamed as: the Gifford Creek Carbonatite Complex (Pirajno et al., 2010). However, due to the mineralogical preponderance of Fe-rich carbonates, Fe-rich silicates and Fe oxides, in some cases almost exclusively (see below), the name of Gifford Creek Ferrocarbonatite Complex (GFC) is considered more appropriate. One of the main features of the GFC is the widespread occurrence of a swarm of ironstone (mainly magnetite, hematite and goethite) veins that are spatially associated with the ferrocarbonatite intrusions (Pirajno and González-Álvarez, 2013). These are surrounded by relatively narrow haloes of fenitic alteration, and are locally associated with quartz veins, interpreted to have formed during post-magmatic alteration processes.

3. Methodology

Field observations were integrated with petrographic studies using conventional optical microscopy, scanning electron microprobe (SEM), Electron Probe Microanalyser (EPMA), X-ray diffraction (XRD), whole-rock geochemistry by XRF and Inductively Coupled Plasma-Mass Spectrometry (ICP-MS), in-situ U–Pb and U–Pb–Th age determinations of apatite and monazite grains from the ferrocarbonatite and fenitic wallrocks, respectively, were carried out, using Laser Ablation (LA) ICP-MS.

3.1. Scanning electron microprobe (SEM)

SEM was carried out on six polished thin sections using a JEOL JSM-6400 SEM (housed at the Centre for Microscopy, Characterisation and Analysis at the University of Western Australia), and configured with Link ISIS energy dispersive (EDS). Mineral identifications were checked and confirmed by semi-quantitative EDS. Operating conditions used were an accelerating voltage of 15 kV and a beam current of 5 nA.

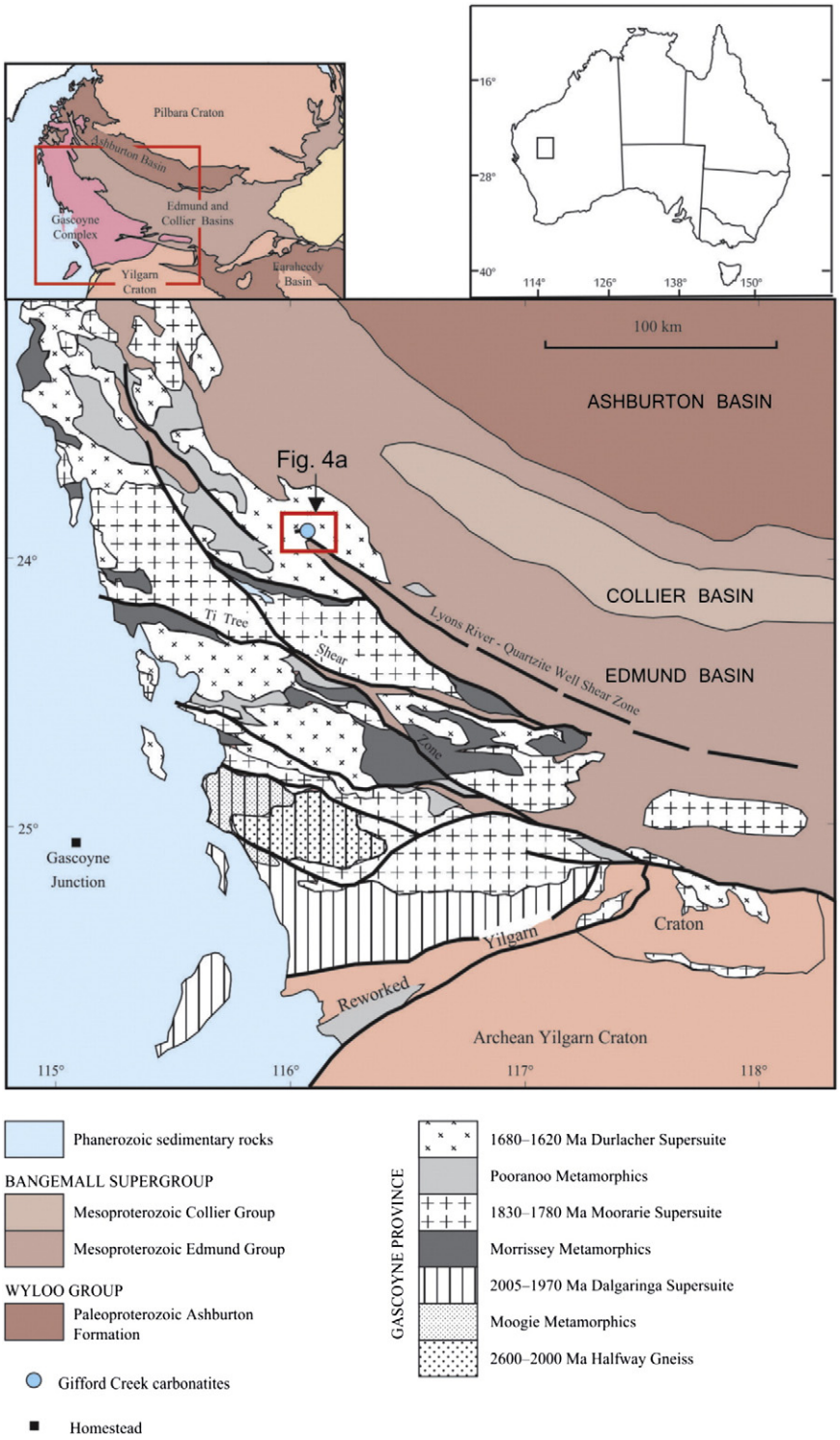

Fig. 1. Regional geological setting of the Gascoyne Province, showing area of Fig. 4. Modified after Sheppard et al., 2010.

The SEM was used to characterise the mineral morphology and composition in the above sample suite. Mineral identification was facilitated using XPLOT® search-match software (http://www.ccp14.ac.uk/solution/search-match.htm).

3.2. Electron Probe Microanalyser (EPMA)

The data were collected using a JEOL 8530F Hyperprobe Field Emission Gun Electron Probe Microanalyser (EPMA), fitted with five wavelength dispersive spectrometers, at the Centre for Microscopy, Characterisation, and Analysis at the University of Western Australia. Operating conditions for sample 197987 were 20 kV accelerating voltage, 50 nA beam current and 5 μm beam size. Operating conditions for sample 197996 were 15 kV accelerating voltage, 20 nA beam current and 2 μm beam size.

Standards used for sample 197987 analysis were Pyrite (Fe), Cassiterite (Sn), Rutile (Ti), Periclase (Mg), Y (Y), $ScPO_4$ (Sc), Scheelite (W), Manganotantalite (Ta), Mn (Mn), Zr (Zr), U (U), and Nb (Nb).

Operating conditions were 20 kV accelerating voltage, 50 nA beam current and 20 μm beam size; whereas standards used for 197996 analysis were $LaPO_4$ (P), Barite (Ba), Celestite (S), Cr_2O_3 (Cr), Magnetite (Fe), Jadeite (Na), Rutile (Ti), Tugupite (Cl), Wollastonite (Ca, Si), Durango Apatite (F), Orthoclase (K), Kakanui Pyrope (Al), Spessartine (Mn) and Springwater Olivine (Mg). Operating conditions were 15 kV accelerating voltage, 20 nA beam current and 10 μm beam size. Results are shown in the Appendix.

3.3. X-ray diffraction

For X-ray powder diffraction analysis (XRPD), rock thin section offcuts were examined using a stereoscopic microscope and sub-samples were obtained by abrading the surface with a tungsten carbide pencil. Resulting powders were further pulverized and mounted on quartz plates for XRPD. For energy dispersive X-ray analysis (EDX), the chemical composition of mineral grains was determined by analysis of carbon-coated polished thin sections using a (CamScan CS3200 LV) SEM connected to an (Oxford INCA) energy-dispersive X-ray analyser.

3.4. Whole-rock geochemistry: major and trace elements

Three samples of ferrocarbonatite were analysed for ten major elements by X-ray fluorescence spectrometry (XRF), and 53 trace elements, including REE and HFSE, using ICP-MS, and Instrumental Neutron Activation Analysis (INAA). Analyses were carried out at Activation Laboratories Ltd. of Ancaster, Ontario, Canada.

Samples were pulverized in a mild steel mill to avoid key trace element contamination (Actlabs Analytical Protocols, 2013). Major oxides were analysed by XRF. Standard deviations for analysis of these elements are as reported by Ackerman et al. (2009).

To address potential problems stemming from incomplete dissolution of refractory minerals, samples were fused with lithium metaborate/tetraborate. The fused sample bead was digested in nitric acid solution. This sample preparation ensures complete digestion of all the refractory mineral phases, and therefore the complete digestion of rare earth elements (La, Ce, Pr, Nd, Sm, Eu, Gd, Tb, Dy, Ho, Er, Tm, Yb and Lu) and high field strength elements (Zr, Hf, Nb, Ta, Ti, Th and U). Internal standards of Activation Laboratories Ltd. were run as well as blanks and duplicates to ensure quality control data. Analytical codes for detailed description of analytical protocols are: 4C, 4LITHO and 4B-INAA (http://www.actlabs.com/, August 2013).

3.5. Apatite dating

In situ U–Pb age determination of apatite grains by LA-ICP-MS on a sample (No. 205577) of ferrocarbonatite was performed, as detailed below. Analysis of the apatite grains was obtained by using a UP213 nm laser ablation system coupled to a Thermo-Finnigan Element2 sector field high resolution ICP-MS at the University of Notre Dame (Indiana, USA). Details of the instrument parameters and conditions used for the in situ U–Pb age determination are furnished in Chen and Simonetti (2013). The analytical protocol employed is similar to that outlined in Simonetti and Neal (2010). A gem quality Madagascar apatite (Thomson et al., 2009) was used as the external standard in the 'standard-sample bracketing' technique in order to monitor instrument drift and laser induced elemental fractionation (LIEF).

Apatite sample and standard grains were laser ablated using a 55 μm spot size and corresponding fluency of ~3 J/cm^2 and repetition rate of 5 Hz. Data acquisition typically consisted of the first ~30 s for measurement of the background ion signals, followed by 30 s of ablation, and a

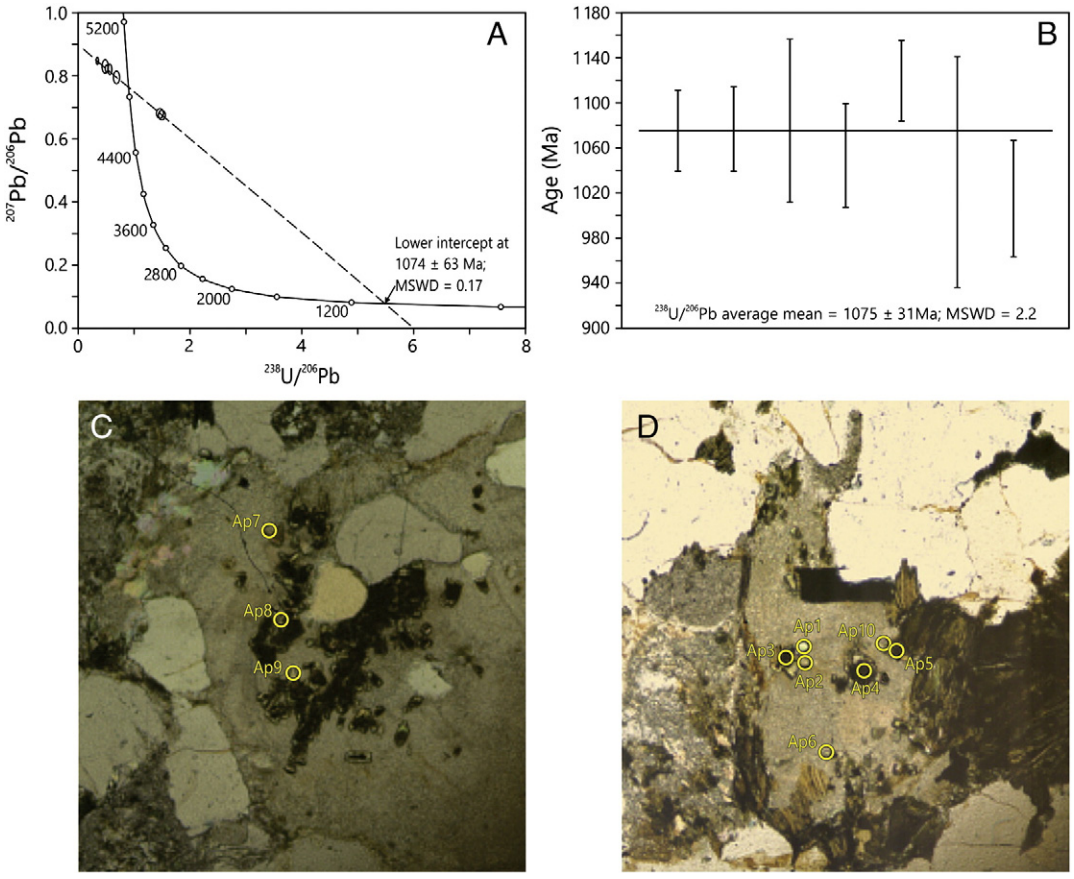

Fig. 2. (A–B) Tera–Wasserburg diagram and weighted mean $^{206}Pb/^{238}U$ age plot for the apatites from a ferrocarbonatite. (C–D) Analytical maps for the in-situ U–Pb age determination (sample 205577). Only the results taken from the fresh apatite spots are used for the age calculation in A and B (i.e. with the exception of Ap3, Ap4, Ap5).

minimum 15 s of washout time. The following ion signals were acquired: ^{202}Hg, ^{204}(Pb + Hg), ^{206}Pb, ^{207}Pb, ^{208}Pb, ^{232}Th, ^{235}U, ^{238}U and ^{232}Th^{16}O. ^{202}Hg was measured to monitor the ^{204}Hg interference on ^{204}Pb (using a ^{204}Hg/^{202}Hg value of 0.229883; Simonetti and Neal, 2010).

Apatite is an accessory U-bearing mineral that contains a significant amount of common Pb (Chen and Simonetti, 2013; Chew et al., 2011). Correction for the common Pb component involved a U–Pb age determination approach that does not require knowledge of the accurate abundance of ^{204}Pb; this is the ^{207}Pb method and was employed for various common Pb-bearing accessory minerals in a number of studies (see Chen and Simonetti, 2013 and references therein). In the ^{207}Pb method, the common lead isotopic composition is determined by projecting the uncorrected data on a Tera–Wasserburg diagram (^{238}U/^{206}Pb vs. ^{207}Pb/^{206}Pb; Tera and Wasserburg, 1972), with the y-intercept delineating the ^{207}Pb/^{206}Pb ratio for common lead. It can then be used to apply a common lead correction to the measured ^{206}Pb/^{238}U ratios using well established common lead–radiogenic lead mixing equations (e.g., Chew et al., 2011; Cox and Wilton, 2006; Simonetti and Neal, 2010). All Tera–Wasserburg diagrams and weighted mean ^{206}Pb/^{238}U ages reported here were determined with IsoPlot v3.0 (Ludwig, 2003). Fragments of Emerald Lake and Durango apatites are used as secondary apatite standards, and both are well characterised with ages of 90.5 ± 3.1 and 30.6 ± 2.3 Ma (Chew et al., 2011), respectively. Repeated analyses of these two standards obtained throughout the study yield ages of 92.6 ± 1.6 and 31.9 ± 1.3 Ma, respectively, and both are identical to the ages reported by Chew et al. (2011). This result in turn serves to validate the analytical methods employed here.

The U–Pb geochronological data of the apatites from the GFC are shown in Fig. 2 and U–Pb ratios in Appendix I. The U–Pb LA-ICP-MS of the GFC apatites yielded an average age of 1075 ± 35 Ma (MSWD = 2.2). Tera–Wasserburg diagram gives the same intercept age of 1074 ± 63 Ma given their associated uncertainties. Of note, this age is well within the range of ages, as well as the area, of the Warakurna LIP (~1078–1070 Ma; see below).

3.6. Monazite U–Pb–Th dating

Monazites from two samples (186707 and 197996) of fenitic rocks associated with ironstone veins were dated using the U–Pb–Th method

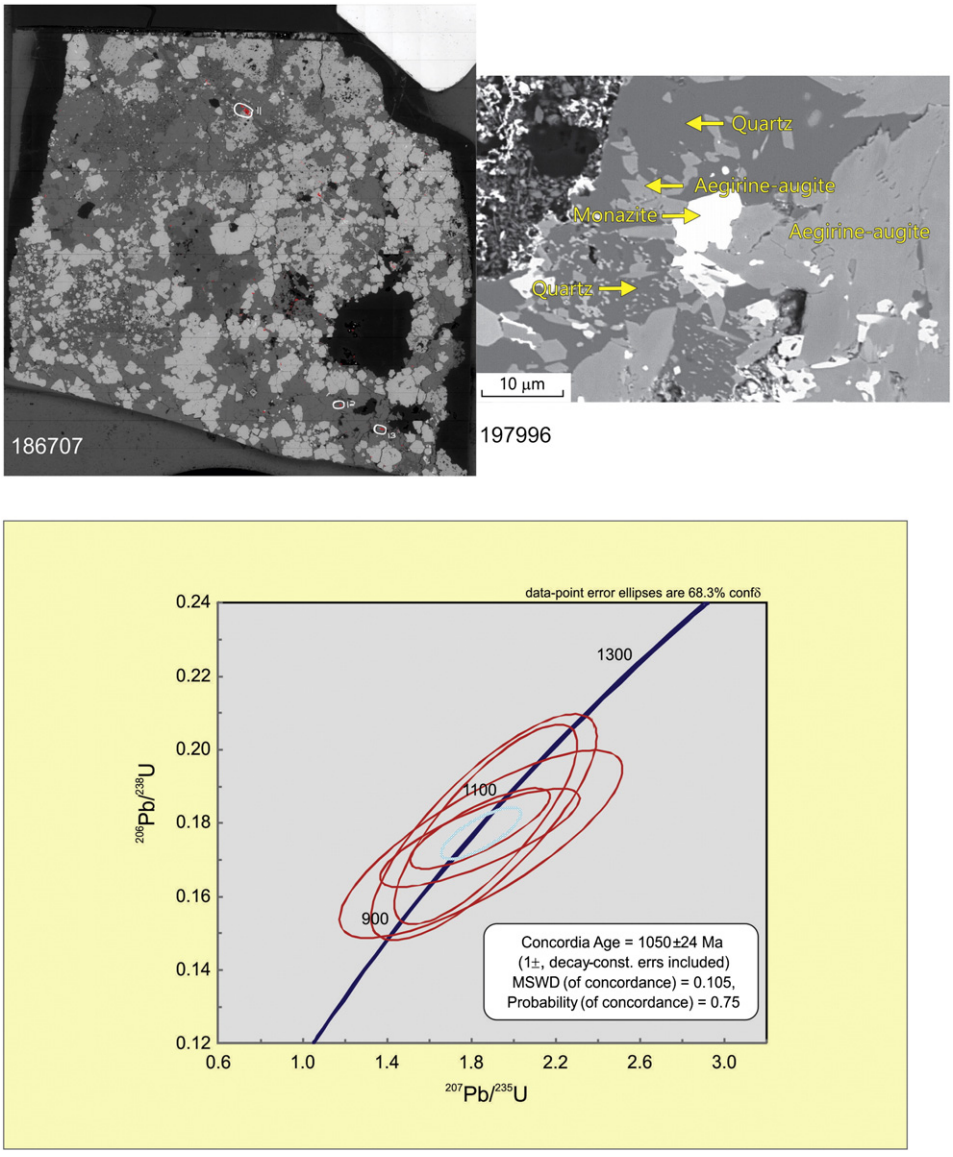

Fig. 3. Sample 186707 (showing analysed spots) at left and SEM of sample 197996 at right with dated monazites; total analysed spots from both samples are 12; concordia age diagram in bottom panel.

by LA-ICP-MS at Queens University. Details of the two samples are given below.

The petrography of the two dated samples is as follows. Sample 197996 is a fenite with a mineralogical association of K-feldspar, sodic pyroxene (aegirine–augite), quartz, alkali amphibole (?), and accessory amounts of monazite, barite, celestite, and zircon. Minerals show an intensive alteration by iron oxides and element exsolution in the K–Na–Ca feldspar series and sodic pyroxenes (aegirine–augite). Abundant heavy mineral inclusions in feldspars and pyroxenes of <15 μm size comprise monazite, zircon, barite and celestite. Sample 186707 is from a 15 cm-thick Fe oxide vein flanked by fenitic alteration cutting through a megacrystic granite of the Durlacher Supersuite. The fenitic halo consists of a phlogopite ± quartz assemblage, with irregular zones of acicular riebeckite, overprinted by Fe oxides (hematite and magnetite). SEM analyses of this sample showed monazite, ferrocolumbite, a single grain of galena and an unidentified Ce–La oxide.

The dating method used is discussed below and analytical details are given in Appendix III (in supplementary table).

The thin sections were then loaded into an Excimer laser (193 nm), and a few of the most likely candidates were ablated. The ablated minerals contained no uranium and it was determined that the grains thought to be monazite must have been a different phase.

The slides were then examined using a FEI-MLA Quanta 650 FEG-Environmental Scanning Electron Microscope, and all mineral phases were indexed using the MLA. The patterns for monazite and zircon were selected and overlaid with a back-scattered electron image of the samples. Using this map, the mineral grains were plotted onto the slides using the Laser Ablation software for the Excimer.

Identified monazites and zircons were ablated using the Excimer at 50% power, 50 Hz repetition rate, 50 μm spot size, 30 s dwell time, and a fluence of 5.9 J/cm^2. The zircon 91500 was used as a standard, and was ablated under the same conditions.

The resulting signal was analysed for U, Th, Hg, Pb, and UO using a Thermo-Fisher Element 2 XR with 0.9 L/min Ar sample gas flow and 0.9 L/min He gas flow (carrier gas) at low resolution (R = 300). Hg202 was used to calculate Hg204 signal and a correction to Pb204 was made. Samples were also blank-subtracted using a gas blank prior to each analysis.

The data were processed manually using Excel and plotted using IsoPlot. A total of 12 spots were analysed in the two samples and the results of this dating exercise are shown in the Concordia plot of Fig. 3, yielding an age of 1050 ± 24 Ma (1σ decay constant error included).

4. The Gifford Creek Ferrocarbonatite Complex (GFC)

4.1. Introduction and previous work

The GFC comprises sills, dykes, and veins of ferrocarbonatite intruding the Pimbyana Granite and Yangibana Granite of the Durlacher Supersuite and metasedimentary rocks of the Pooranoo Metamorphics (Fig. 4). The ferrocarbonatites are associated with complex and irregularly distributed zones of fenitic alteration. Also associated with the carbonatites and fenites are veins of Fe oxides (magnetite, hematite and goethite) and quartz that were likely formed during post-magmatic alteration processes, by dissolution of Fe carbonates (see below).

The ferrocarbonatite sills and dykes form a NW-trending belt in the south-western sector of the GFC (Fig. 4), parallel to, and to the north of the Lyons River Fault. On the northern side of this NW-trending belt are swarms of carbonatite and ironstone veins, distributed in a series of sinuous trends, terminating along a WNW-trending belt of carbonatite–ironstone veins. This WNW-trending belt is along a poorly defined lineament, which Pearson et al. (1996) called the Bald Hill Lineament, which may represent one side of a pull-apart structure (see Discussion). The granitic country rocks north of the Bald Hill Lineament are extensively hydrothermally altered, as indicated by nearly pervasive replacement of the primary igneous minerals by green biotite, epidote and calcite. However, it is not clear if this alteration is related to the fenitic alteration associated with the carbonatites. At the Spider Hill locality (Fig. 4A) there are narrow dykes and flat-lying sills of ferrocarbonatite, which intrude the Pimbyana Granite. These are surrounded by fenitic haloes, whose mineralogy is dominated by aegirine, apatite, phlogopite, magnetite and pyrochlore (Pearson et al., 1996).

Pearson (1996), Pearson and Taylor (1996) and Pearson et al. (1996) reported on the nature, petrography and mineral chemistry of various rocks from the GFC, which they called Lyons River ultrabasic sills. These workers recognised the extensive fenitisation of the granitic country rocks of the Gascoyne Provinces and also pointed out that the GFC represents the largest complex of its kind in Australia, occupying an area of about 700 km^2 (Fig. 4A; see below).

Flint and Abeysinghe (2000) recorded rare earth elements and uranium mineralisation in the ferrocarbonatite and ironstone veins and quoted estimated combined resources of 3.5 Mt, averaging 1.7% REE oxides. Recent drilling by Hasting Rare Metals Ltd. at Yangibana reported low grades of the Heavy Rare Earth Oxides (HREOs), but of particular interest is the high Nd grade, which averages around 0.4 wt.% Nd_2O_3, or 24% of the Total Rare Earth Oxides (TREO; Hastings Rare Metals Ltd., 2012).

4.2. Ferrocarbonatite intrusions

Our petrographic, XRD and SEM investigations, combined with those of Pearson and her co-workers, show that the ferrocarbonatites are dominantly composed of ankerite, dolomite, magnetite, Fe–Ti oxides, and arfvedsonite–riebeckite, with variable proportions of perovskite, pyrochlore, ferrocolumbite, phlogopite, calcite, apatite, barite and monazite (Fig. 5); EPMA analyses of ferrocolumbite grains in sample 197987 and those of amphiboles in sample 197996, are given in Appendix II.

The sills and dykes north of the Lyons River Fault are characterised by a carbonate-rich matrix, containing fluoroapatite, celestite, bastnaesite, phlogopite, barite and monazite. Our field and petrographic work shows that these rocks are generally ankeritic carbonatites and locally silicocarbonatite (arfvedsonite-rich). Fig. 6 shows some of the field features of these ferrocarbonatitic rocks, whereas some of the key petrographic features are shown in Fig. 7.

An important aspect is that many samples, if not all, contain more than 50% by volume of Fe-rich carbonate (ankerite) and silicate mineral phases (Na–Fe amphibole, phlogopite, as well as primary Fe oxides (magnetite)) and lesser amounts of dolomite and calcite, which places the nomenclature of these rocks in the carbonatite field (Le Maitre, 2002) and more specifically ferrocarbonatite (Gittins and Harmer, 1997). Remarkably, in one sample of ferrocarbonatite, millimetre scale banding exhibits features that we interpret as due to a quench-textured silicate–carbonate immiscibility (Fig. 8). Immiscibility of two liquids, carbonate–silicate, has been experimentally investigated and observed in a number of alkaline complexes in East Africa and Italy (e.g., Freestone and Hamilton, 1980; Kjarsgaard and Hamilton, 1989; Kjarsgaard and Peterson, 1991; Solovova et al., 2005; Stoppa et al., 2005).

The fenitic haloes surrounding the carbonatites are mostly characterised by the presence of feldspars and/or alkali-amphiboles and magnetite. Alkali amphibole has compositions ranging from potassian magnesio-arfvedsonite to magnesio-riebeckite. The amphiboles in the fenitic rocks contain F ($KNa_2Mg_4Fe^{3+}Si_8O_{22}F_2$) and are classified as potassium magnesio-fluor-arfvedsonite (Pearson and Taylor, 1996). Sodic pyroxene is generally aegirine with a high $NaFe^{3+}Si_2O_6$ component and with TiO_2 contents of up to 4 wt.%. Mica is metasomatic and is Al-deficient fluorphlogopite (F contents from 1.5 to 4.5 wt.%; Pearson and Taylor, 1996). Fenitic alteration is mostly spatially associated with the carbonatites, but it can also form discrete veins and veinlets in basement granitic rocks (Pimbyana and Yangibana Granites; Fig. 9). Fenitic alteration is described in more detail below.

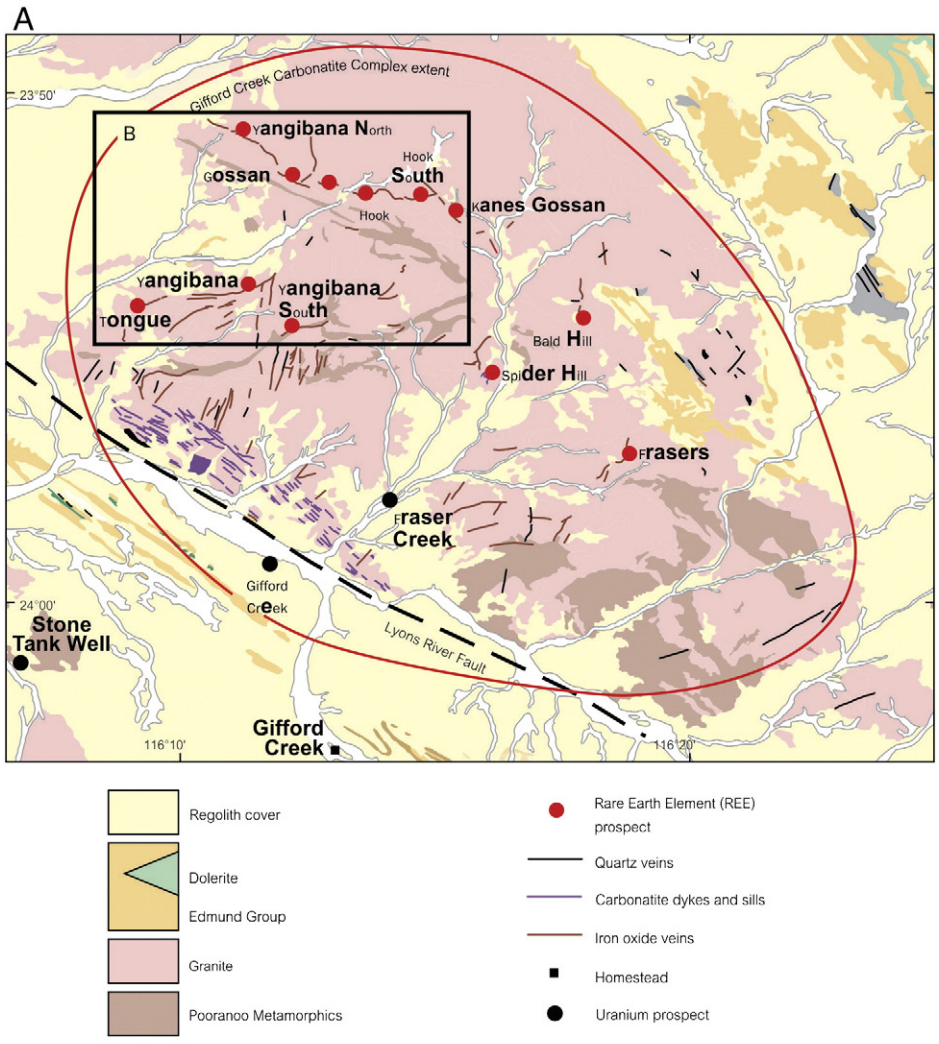
A
Gifford Creek Carbonatite Complex extent
23°50'
B
Yangibana North
Hook South
Gossan
Hook
Kanes Gossan
Yangibana
Yangibana South
Tongue
Bald Hill
Spider Hill
Frasers
Fraser Creek
Gifford Creek
24°00'
Stone Tank Well
Lyons River Fault
116°10'
Gifford Creek
116°20'
Regolith cover
Dolerite
Edmund Group
Granite
Pooranoo Metamorphics
Rare Earth Element (REE) prospect
Quartz veins
Carbonatite dykes and sills
Iron oxide veins
Homestead
Uranium prospect

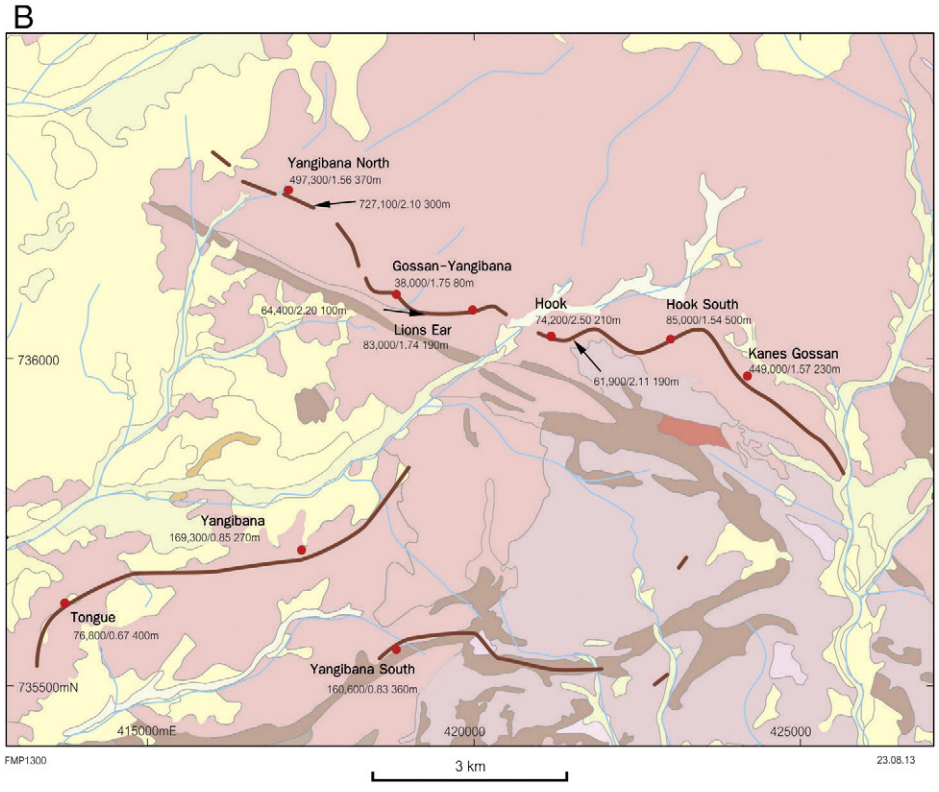
B
Yangibana North
497,300/1.56 370m
727,100/2.10 300m
Gossan-Yangibana
38,000/1.75 80m
64,400/2.20 100m
Lions Ear
83,000/1.74 190m
Hook
74,200/2.50 210m
Hook South
85,000/1.54 500m
61,900/2.11 190m
Kanes Gossan
449,000/1.57 230m
736000
Yangibana
169,300/0.85 270m
Tongue
76,800/0.67 400m
Yangibana South
160,600/0.83 360m
735500mN
415000mE
420000
425000
FMP1300
3 km
23.08.13

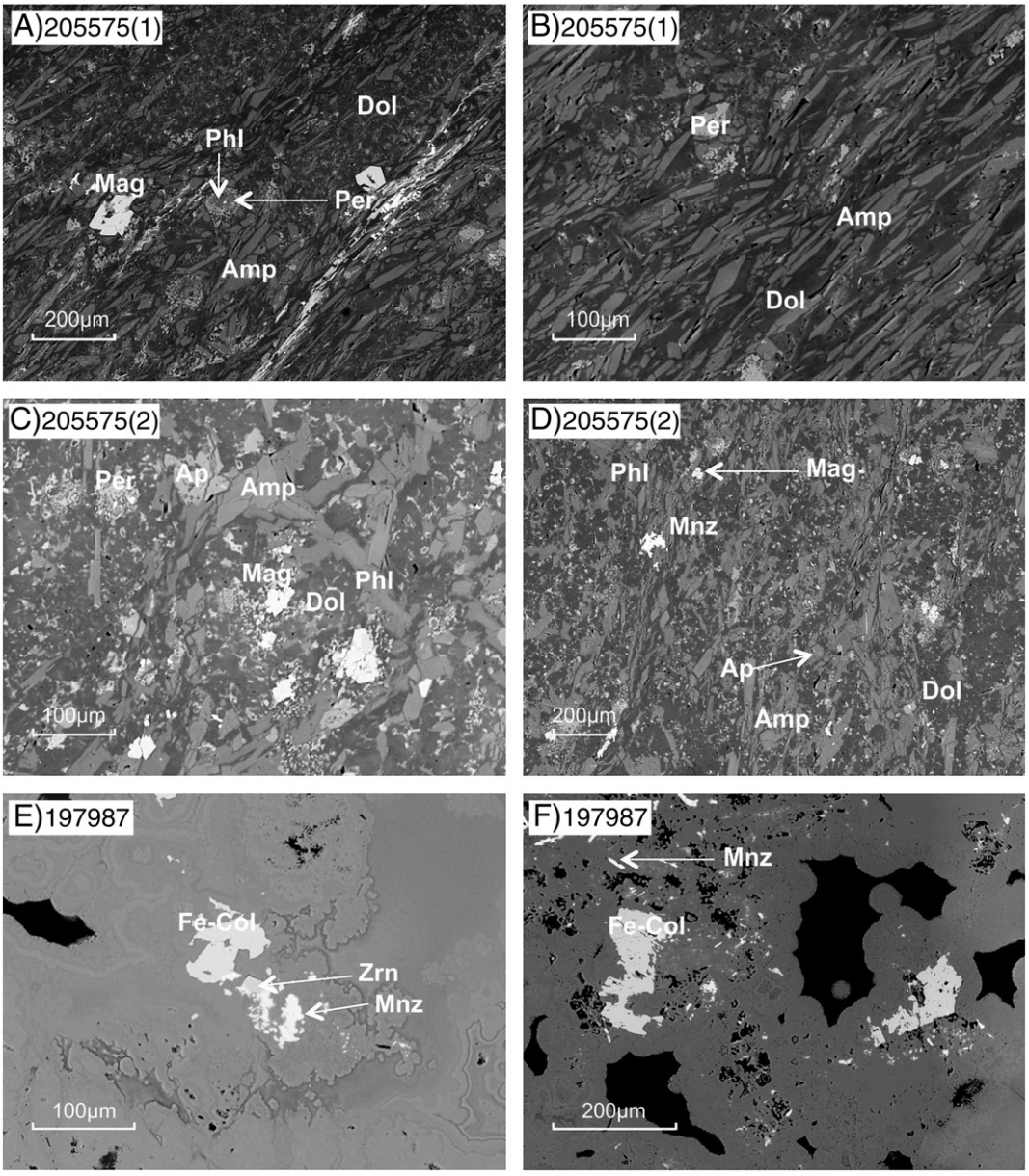

Fig. 5. A), B), C) and D) SEM photomicrographs, showing main mineralogical assemblages. A) and B) for Section 1 of 205575 sample has 24% ankerite-dolomite (Dol), 22% amphibole (Amp), 5% perovskite (Per), 5% phlogopite (Phl), 1% magnetite (Mag), <1% barite (not shown) and <1% manganosite; whereas Section 2 for the same sample displays 40% amphibole, 30% ankerite-dolomite, 20% phlogopite and <1% monazite (Mnz); (E) Backscattered electron photomicrographs showing ferrocolumbite (FeCol), zircon (Zrn) and (F) a grain of ferrocolumbite with monazite.

4.3. Ironstone veins

To the north of the ferrocarbonatite belt, there are numerous sinuous ferrocarbonatite veins associated with ironstone veins and pods (Fig. 4), enclosed or surrounded by zones of fenitisation of the country rocks (Pimbyana Granite and other granitic units of the 1680–1620 Ma Durlacher Supersuite (Sheppard et al., 2007, 2010)). The ironstone veins, with dominant N, NE and WNW trends (Fig. 4), consist of magnetite, hematite and supergene goethite.

Exploration drilling indicated that some of these ironstones can be traced at depth to narrow (5–10 m thick) ferrocarbonatite dykes (Newcrest Mining Ltd., 1991). This was also recognised by Pearson et al. (1996) and confirmed by our field observations, whereby the ferrocarbonatite sill-like and dyke intrusions locally exhibit a gradual transition to Fe oxides.

The ironstone veins, associated with carbonatites are one of the main features of the GFC (Pirajno and González-Álvarez, 2013). The veins are characterised by sinuous or arcuate trends and locally occur as pods of Fe oxides and are generally between a few centimetres and 10 m thick (Figs. 9 and 10). Veins of hematite–magnetite, in places with supergene alteration to massive goethite, are locally associated with quartz veins (Fig. 4). The presence of quartz and/or calcite is attributed to later hydrothermal activity, distinct from the effects of Fe-oxide rich and fenitising fluids. Attitude, field relationship, and petrographic

Fig. 4. (A) Simplified geological map of Gifford Creek Ferrocarbonatite Complex, showing ironstone veins, dykes and NW-trending belt of ferrocarbonatite dykes and sills (formerly called Lyons River ultrabasic sills; Pearson and Taylor, 1996; Pearson et al., 1996); also shown are the main REE prospects investigated by drilling. (B) Sketch map showing distribution of the mineral prospects, with defined resources (tonnes/%TREO/length in metres) owned by Hastings Rare Metals Ltd. (image courtesy of Andy Border of Hastings Rare Metals Ltd.).

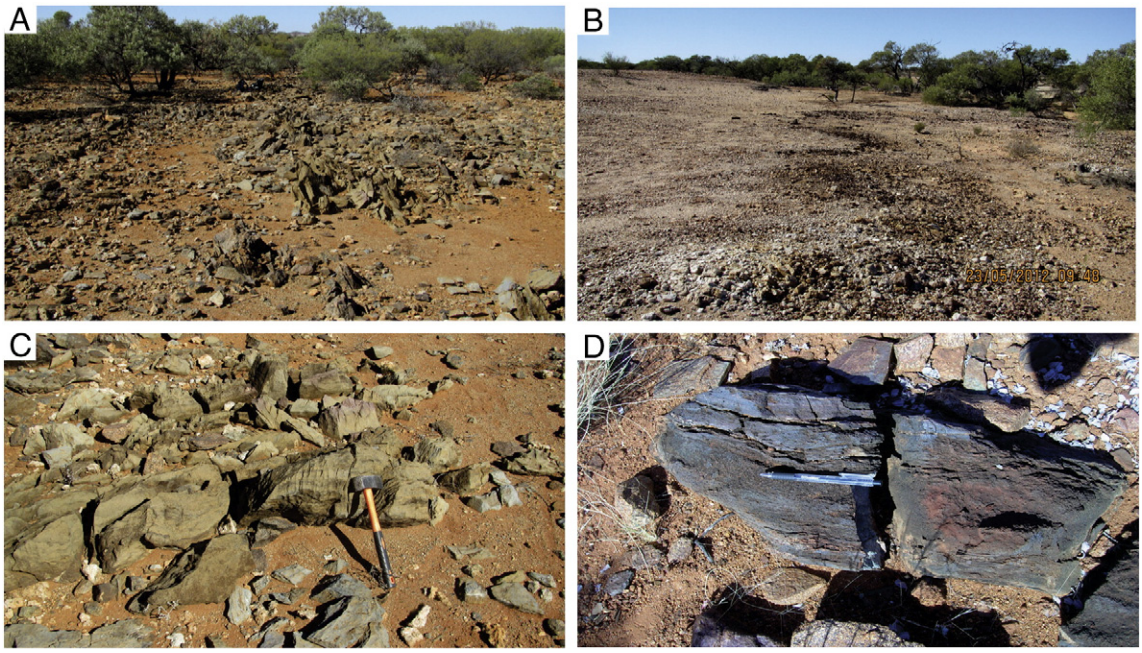

Fig. 6. Field features; A) and B) massive to flow-banded ferrocarbonatite dyke about 100 m long and intruding Pymbiana granite, in B note metre-scale sinuosity of the dyke; C) dissolution pits in ferrocarbonatite; D) flow-banded ferrocarbonatite, surface covered in Fe oxides derived from the breakdown of the Fe carbonates; E) detail of ferrocarbonatite partly replaced by Fe oxides; and F) carnotite staining of partially oxidized ferrocarbonatite.

data suggest that the ironstone veins post-date the emplacement of the ferrocarbonatite intrusions. The petrography of two selected samples of ironstone is described below.

Sample 197986 is composed of magnetite, barite and monazite in a matrix of hematite + goethite. The magnetite occurs as large phenocrysts up to 1 mm size. Fractions of <15 μm size comprise euhedral

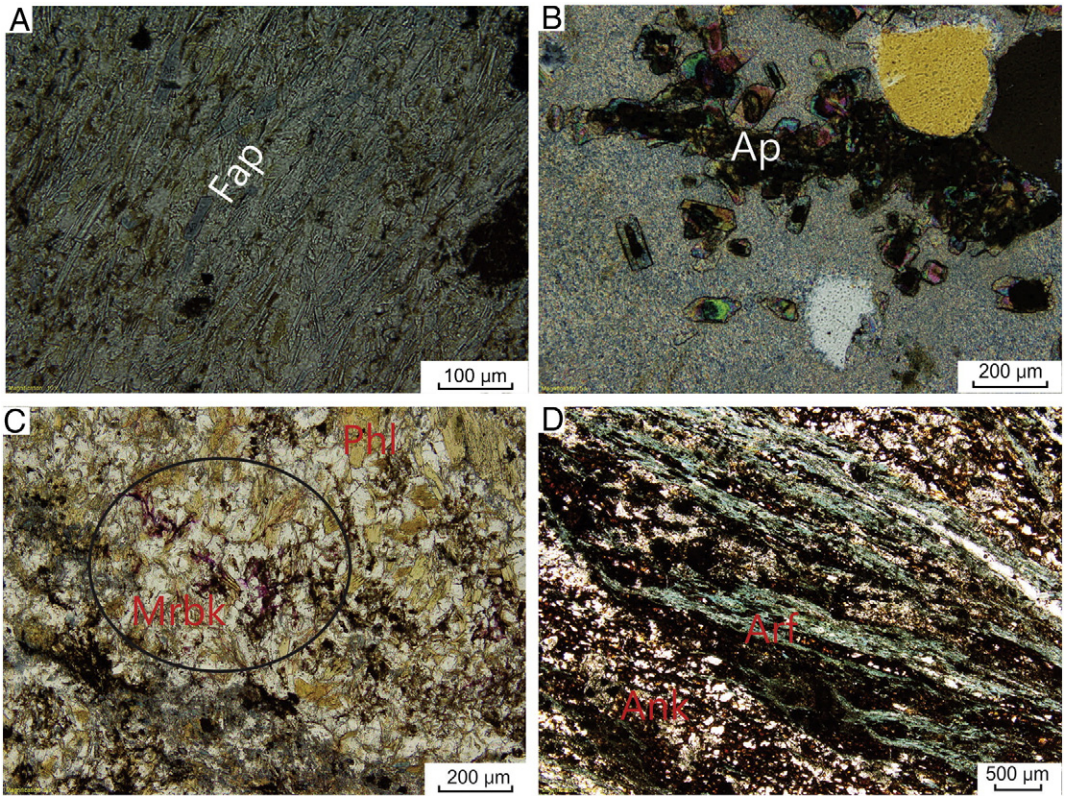

Fig. 7. Photomicrographs in plane polarized light of selected samples from the WNW-trending ferrocarbonatite intrusions north of the Lyons River Fault; A) fluoroapatite acicular crystals aligned along the flow-banding of ferrocarbonatite; B) apatite crystals in crypto-crystalline carbonate material (dated sample); C) Ferrocarbonatite assemblage of mostly dolomite, overprinted by phlogopite and magnesio-riebeckite (anomalous purple colour in circle); D) flow-banded Fe carbonate (probably ankerite) and dolomite partially overprinted by Fe oxides, and arfvedsonite. Mineral abbreviations (based on Whitney and Evans, 2010): Dol, dolomite; Pcl, pyrochlore; Arf, arfvedsonite; Cal, calcite; FAp, fluoroapatite; Ank, ankerite; Rbk, riebeckite; Mrbk, magnesio-riebeckite; Phl, phlogopite; Ap, apatite; Mag, magnetite.

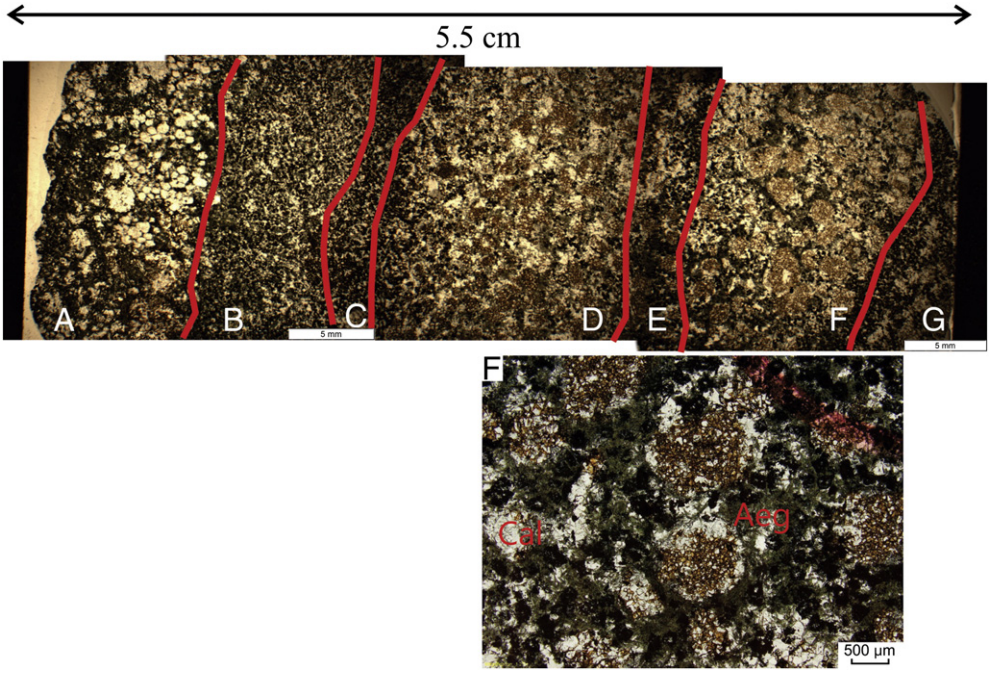

Fig. 8. Sample displaying banded carbonatite at thin section scale. A) Calcite-arfvedsonite; B) Fe-carbonate-arfvedsonite; C) Dominantly Fe carbonate and Fe oxides; D) Fe carbonate-calcite-arfvedsonite; E) Dominantly arfvedsonite; F) Fe-carbonate-calcite-arfvedsonite; G) globular Fe-carbonate-calcite-arfvedsonite. A photomicrograph of (F) is shown below, in which partially oxidized Fe carbonate globules are set in a matrix of acicular aegirine and calcite; this texture is interpreted as due to immiscible carbonate-silicate liquids (see text for more details).

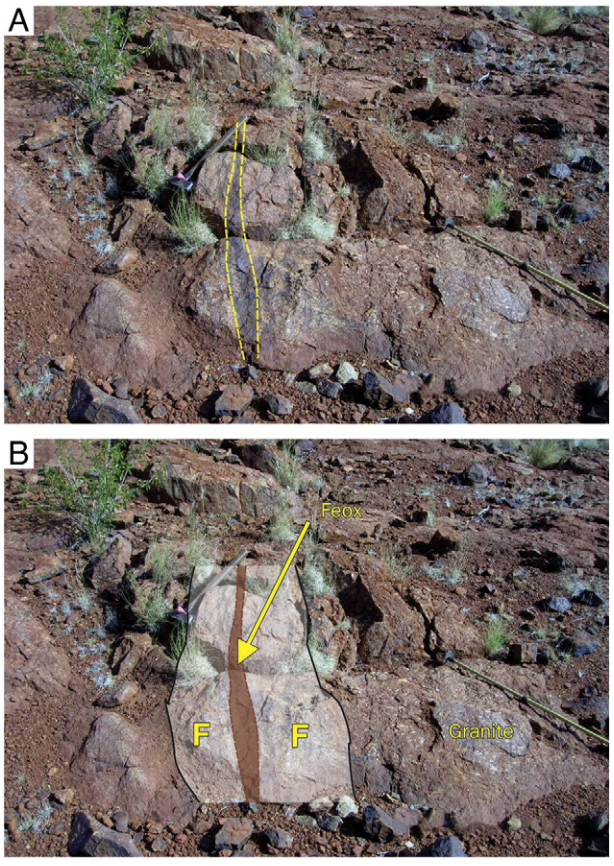

Fig. 9. (A) Outcrop showing an iron oxide vein cutting through a granite outcrop; B) shows the extent of the fenitic alteration halo (F) and the Fe oxide (Feox) vein in the outcrop.

barite and rounded monazite grains disseminated in the hematite + goethite matrix. All mineral phases are severely affected by secondary Fe-oxide (goethite–hematite) alteration. Sample 197987 contains abundant barite and rounded monazite grains disseminated in a matrix of amorphous Fe oxide (with some traces of mica). Barite grains are commonly larger than 100 μm and with a skeletal texture, reflecting severe corrosion of the original barite. All mineral phases are affected by varying degrees of Fe-oxide alteration. The textural features of the carbonatite protolith have been obliterated leaving an insoluble fraction of bastnaesite, pyrochlore, ferrocolumbite and monazite grains.

Mineral exploration drilling has shown that these veins have very shallow (~10°) to steep (~65°) dips (Pooley, 1989). The ironstone veins have variable trends, although in many instances they tend to be almost perpendicular to the trend of the ferrocarbonatite swarm of sills and dykes that runs sub-parallel to the Lyons River Fault, on the southern margin of the GFC (Fig. 4A). Pearson et al. (1996) reported the presence of magnetite pods (which are part of the ironstones) grading into narrow, flat-lying aegirine–apatite–phlogopite–magnetite–pyrochlore sheets. As shown in Fig. 4B, some of the ironstones have been investigated for their rare earth elements (REE) and U mineral potential in a number of localities, such as the Yangibana North and South, Yangibana, Spider Hill, Fraser, Lions Ear, Hook and Hook South, Kanes Gossan and Tongue (Pirajno and González-Álvarez, 2013). These were investigated by field mapping and shallow drilling by mineral exploration in the 1970s and 1980s (Gellatly, 1975; Hoatson et al., 2011; Pearson, 1996; Pearson et al., 1996; see also Fig. 2). Recently, renewed interest, particularly in the Yangibana prospect is linked to their REE, U and Th potential.

As mentioned above, exploration drilling shows that the ironstones grade at depth to ferrocarbonatite rocks which, in addition to ankerite and dolomite, contain variable amounts of magnetite, ferroan phlogopite, apatite, allanite, pyrite, sodic amphibole and aegirine. Monazite, pyrochlore, bastnaesite, melilite, cancrinite and lamprophyllite are present as accessory minerals. Traces of fluorite, sphalerite, molybdenite and galena were reported by Pearson et al. (1996).

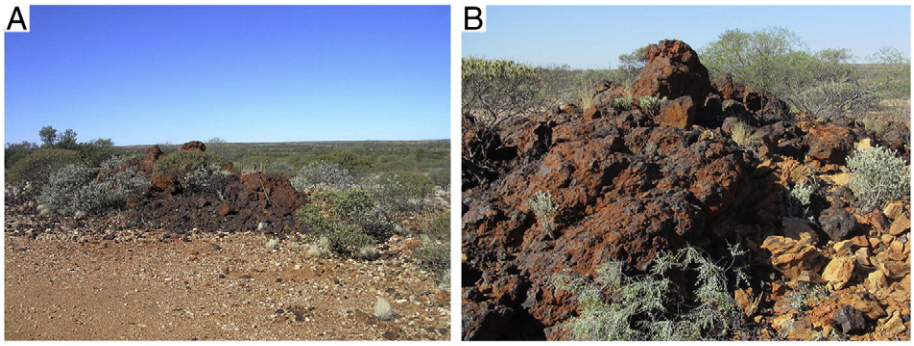

Fig. 10. Typical outcrops of ironstone veins, A) Yangibana prospect and B) Tongue prospect; see Fig. 4.

The *Yangibana* ironstone (Fig. 10A) is composed of massive and generally amorphous Fe oxides with patches of relic or second-generation quartz (related to oxidation/weathering). In reflected light microscopy the Fe oxides show at least 3 generations, from earliest to latest: 1) magnetite, 2) hematite replacing magnetite crystals (e.g. cubic), starting along exsolution lamellae, and 3) dull, goethitic (oxyhydroxide) material. The *Tongue* ironstone veins (Fig. 10B) extend for about 400 m with thicknesses of 0.5 to 2.5 m (Pooley, 1989). This ironstone material is associated with fenitised rocks at the footwall, typically showing a cataclastic to fluidised texture, with cloudy feldspars (albite and orthoclase?) within a crushed matrix, and with Fe oxides along grain boundaries and in cross-cutting fractures.

The magnetite in the ironstone veins can be seen to have rims of hematite. Colloform hematite and goethite, more or less banded, locally associated with bright yellow (carnotite?) patches and rims around the Fe oxides. Crude banding is present, which may be related to the original ferrocarbonatite texture, or it may have developed during oxidation and regolith development. Magnetite is euhedral and probably is a primary mineral phase. It is spatially associated with bastnaesite, sodic amphibole and/or cancrinite, which form the matrix between the magnetite crystals. Thus, magnetite–bastnaesite–sodic amphibole–cancrinite is assumed to be part of the carbonatite system. Hematite on the other hand, appears to almost pervasively occupy fractures and cleavage traces, and may locally replace the main ferrocarbonatite and/or fenitic mineral assemblages.

4.3.1. A genetic model for the ironstones of the Gifford Creek Ferrocarbonatite Complex

Based on their morphology and composition, the ironstone veins of the GFC are unusual and to the best of the authors' knowledge the nearest analogue, also cited by Pearson et al. (1996), are the Fe-rich, low-temperature hematite–calcite–dolomite rocks, known as "rødberg" (red rock), which occur in the Fen carbonatite in South Norway (Andersen, 1984). Rødberg refers to disseminated and massive hematite in thin irregular veins, developed along joints and grading into the primary ferrocarbonatite over distances of 2–3 m. The rødberg hematite veins were mined as iron ore in the past. Andersen (1984) proposed that the rødberg was formed by metasomatic alteration of the ferrocarbonatite in zones of fracturing. The rødberg material is seen to replace granular ankeritic ferrocarbonatite, mostly along fractures. However, Andersen (1984) also pointed out that the rødberg was by no means the last stage in the ferrocarbonatite mineral paragenesis, because in one case a ferrocarbonatite body was found to enclose round xenoliths of rødberg. The rødberg replaces pre-existing ferrocarbonatite along fractures, followed by more advanced stages in which the entire ferrocarbonatite is replaced by rødberg. A petrogenetic model, as originally envisaged by Andersen (1984), can be summarised as follows.

The rødberg is initiated by exsolution of hematite from the Fe-bearing carbonate. At the same time, other Fe-bearing phases, such as magnetite, pyrite, and ilmenite are also oxidized to hematite and locally to rutile and sulphate species. Andersen (1984) further suggested that a mobile fluid phase had to be active in order to supply oxygen to the system and remove the soluble oxidation products. The hematite enrichment was brought about by dissolution of the Fe-carbonate present in the ferrocarbonatite and not by external introduction of iron. Furthermore, REE-bearing minerals, such as monazite and synchysite, were unaffected by oxidation and remained in the rødberg.

A somewhat similar petrogenetic model can be envisaged for the Gifford Creek ironstones, as elaborated below. Based on field and petrographic observations described previously, we suggest that fenitisation occurred during and after the emplacement of the carbonatites. This was followed by hydrothermal activity, likely induced by the progressive cooling of carbonatite magma and the release of volatiles, during which dissolution of Fe from primary magnetite, ilmenite and ferrocarbonatite minerals (dolomite, ankerite) took place. An initial stage of comparatively high-T hydrothermal activity produced secondary minerals, such as biotite and phlogopite, commonly observed in the fenitic wallrocks around the ironstone veins. Some of the stages of ferruginisation of the primary ferrocarbonatite and fenitic wallrocks, from early fracture-controlled to pervasive supergene replacement are shown in Fig. 11. A four-stage paragenetic process, which would have led to the formation of the ironstone veins, as seen today has been proposed by Pirajno and González-Álvarez (2013) and described below.

Stage 1 would have been characterised by the dissolution of the ankerite and dolomite, and perhaps the direct conversion of igneous magnetite to form Hematite I, due to reactions, as originally proposed by Andersen (1984):

$$Ca(Mg_{0.6}Fe_{0.4})(CO_3)_2 + 0.1O_2 \rightarrow 0.2Fe_2O_3 + 0.6CaMg(CO_3)_2 + 0.4CaCO_3 + 0.4CO_2$$

$$Fe_3O_4 + H2O \rightarrow Fe_2O_3 + Fe(OH)_2$$

$$2FeCO_3 + 0.5O_2 \rightarrow Fe_2O_3 + 2CO_2.$$

These reactions would require higher temperatures than those usually associated with supergene processes, which are generally driven by weathering at temperatures of less than 50 °C (Taylor and Eggleton, 2001). Hematite from this stage can be seen to have developed along flow lines or laminae of the fluidal ferrocarbonatite (Fig. 11A). In Stage 2, hematite is redistributed across the primary flow textures (Fig. 11B, C). This is followed by the development of supergene hematite of stage 3, which overprints all previous textures (Fig. 11D). The final stage 4, colloform hematite and goethite pervasively replace the Fe oxides of the previous stages, resulting in the observed ironstones (Fig. 11E, F).

4.4. Fenitic alteration haloes

Fenitic alteration which is widespread, laterally extending from a few metres to tens of metres, is spatially associated with the

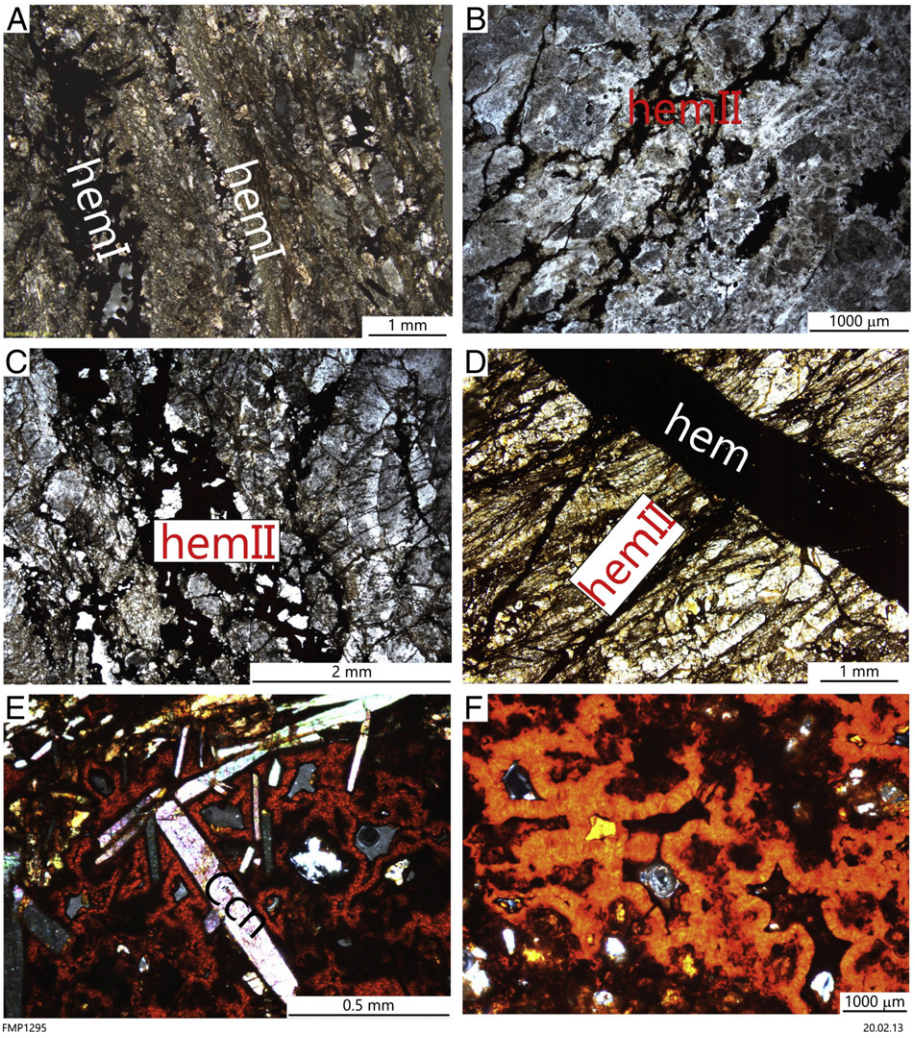

Fig. 11. Photomicrographs in plane polarized light, showing progressive replacement by Fe oxides, (A) hematite I (hemI) developing along flow banding of rheomorphic fenite; (B) and (C) hematite II (hemII) filling microfractures; (D) hematite II cut by a hematite veinlet of a later generation (probably hematite III); (E) and (F) supergene colloform Fe oxides, with relic cancrinite (Ccn) crystals in (E).

ferrocarbonatites sills and dykes as well as the ferrocarbonatite–ironstone veins. These fenitic haloes are best observed in the footwall of the ironstone veins and are characterised by the presence of orthoclase, albite, riebeckite, arfvedsonite, aegirine and magnetite as the main mineral phases, as well as economically important minerals such as monazite, pyrochlore and columbite–tantalite group minerals. Lesser quantities of other minerals in the fenitised rocks include phlogopite mica, cancrinite and lamprophyllite and variable amounts of nepheline and sodalite. In some cases monomineralic feldspar zones are present, with the rock best described as orthoclasite.

The abovementioned minerals that are the main components of fenitic alteration, occur in varying amounts, presumably due to, not only the composition of the alkaline fluids, but also the primary mineralogy of the rocks affected. This results in a great variety of textures and dominant mineralogy. Furthermore, petrological analysis shows that the fenitisation process is highly dynamic and multiphase. For example, there are at least two generations of aegirine-augite/aegirine: coarse grained, and very fine-grained granular aggregates, overprinted by acicular riebeckite (Fig. 12A). In turn, acicular riebeckite is overprinted by phlogopite mica. In the same rock isolated euhedral pyrochlore (Fig. 12B), slightly pleochroic lamprophyllite crystals and stellate aggregates of green–blue riebeckite may also occur. With advancing fenitisation, albite and orthoclase become abundant, with acicular aegirine intergrown with magnesio-arfvedsonite. The feldspathisation of the affected rocks can be pervasive, resulting in rocks that have the appearance of syenites (Pirajno, 2012). A good example at Gifford Creek is furnished by an outcrop of a pervasively fenitised wallrock, possibly a granite of the Pimbyana or Yangibana suites, which resembles a syenite. In the same rock, relic coarse K-feldspar crystals are overprinted by felsitic masses of adularia, associated with growths of radiating needles of arfvedsonite.

Fluidal textures are common in these fenites and generally consist of bands or laminae of alternating fine-grained packed aggregates of K-feldspar and plagioclase (oligoclase-albite compositions) and of pale green biotite. Euhedral magnetite crystals of a later generation are aligned along bands of biotite. The feldspar bands exhibit a granular to fluidal-like texture in places (Fig. 12C). In other cases, assemblages of euhedral nepheline, forming granular aggregates, occur within masses or polycrystalline aggregates of biotite, with distinct green pleochroism and abundant acicular riebeckite (Fig. 12D). Minor chalcedonic silica and/or zeolite minerals fill interstitial spaces or vughs. These latter minerals are attributed to later hydrothermal, possibly meteoric, activity.

An almost pervasively fenitised porphyritic granite (Pimbyana granite?), consists of aggregates of nepheline and sodalite/nosean, with the latter altered to analcime and bluish-green riebeckite, associated with a fluidal/flow texture, where epidote overprints riebeckite. According to the IUGS system, this rock could be a foidolite, however, this is not an igneous rock but wholesale replacement by feldspathoids

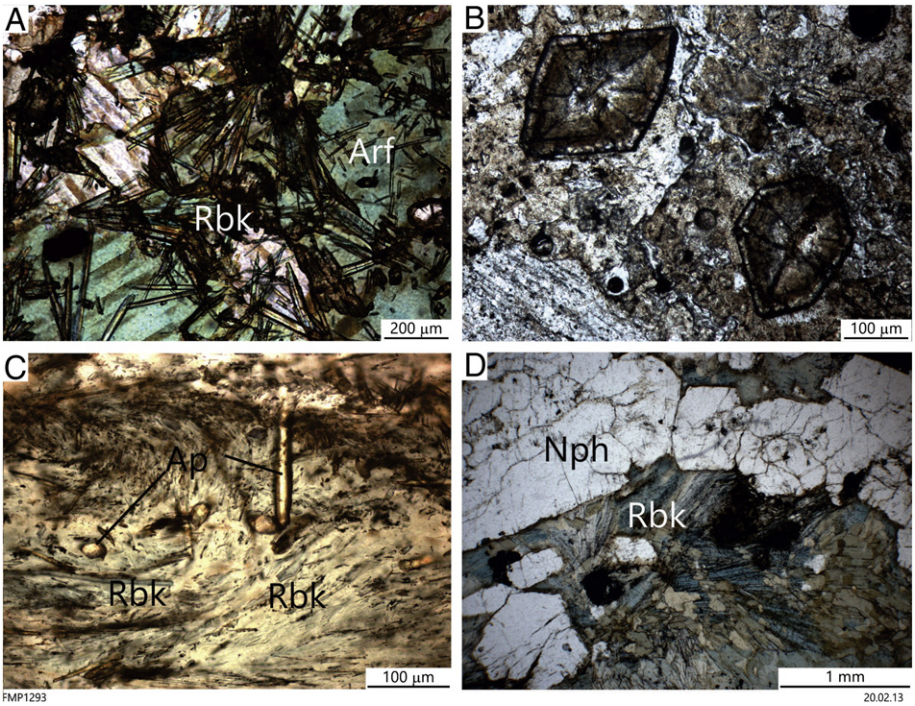

Fig. 12. Photomicrographs in plane polarized light of fenitic wallrocks at footwall of ironstone, A) acicular riebeckite (Rbk), overprinting arfvedsonite (Arf); B) zoned pyrochlore crystals; C) riebeckite and apatite (Ap) crystals in a fluidal texture; D) nepheline (Nph) crystals and acicular riebeckite.

of a pre-existing granitoid, in other words a fenite. Similar fenites are recorded from the Messum Complex in Namibia, where Mathias (1956) noted rocks that were completely replaced with introduction of K-feldspar, amphibole, aegirine-augite, sodalite and analcime. Mathias (1956) referred to these rocks as theralite and he also noted that these fenites had been "mobilized", hence the fluidal/flow texture, seen in these rocks.

An outstanding illustration of a texture relating to fenitising fluids can be seen in Fig. 13A, in which a fractured and coarse-grained albite assemblage is cut by veinlets of phlogopite or biotite. Additionally, interstitial zones of adularia, forming a granular to felsitic aggregate, showing a plumose texture are also present (Fig. 13B, C and D). Two distinct assemblages can be discerned here: 1) coarse grained albite-dominated assemblage (albitite); and 2) fine grained, plumose

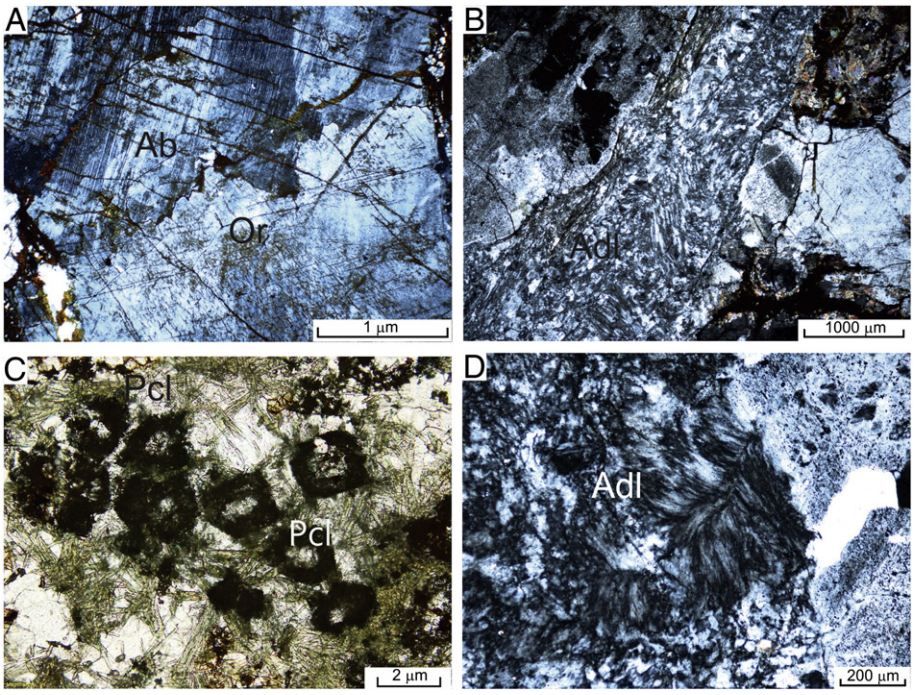

Fig. 13. Transmitted light photomicrographs in crossed polars of fenitic wallrocks at footwall of an ironstone vein. (A) orthoclase (Or) replacing albite (Ab); (B) adularia (Adl) with rheomorphic texture, cutting and replacing albite; biotite is in the top right corner; (C) Fe oxide pseudomorphs of pyrochlore crystals (Pcl), overprinting arfvedsonite acicular crystals and calcite; D) fluidal and plumose adularia.

Table 1
Whole-rock geochemical analysis of selected samples in the Gifford Creek Ferrocarbonatite Complex, Gascoyne Province.

Analyte symbol	Unit symbol	Detection limit	Analysis method	Sample 205575	Sample 205575B	Sample 205576
SiO_2	%	0.01	FUS-XRF	16.91	18.88	45.03
Al_2O_3	%	0.01	FUS-XRF	1.58	2.29	27.45
Fe_2O_3(T)	%	0.01	FUS-XRF	8.02	12.69	9.4
MnO	%	0.001	FUS-XRF	0.329	0.265	0.049
MgO	%	0.01	FUS-XRF	16.88	16.35	2.68
CaO	%	0.01	FUS-XRF	21.26	18.68	0.3
Na_2O	%	0.01	FUS-XRF	0.81	0.87	0.2
K_2O	%	0.01	FUS-XRF	0.29	0.55	9.19
TiO_2	%	0.001	FUS-ICP	2.154	2.245	1.201
P_2O_5	%	0.01	FUS-XRF	0.09	1.5	0.06
Cr_2O_3	%	0.01	FUS-XRF	0.05	0.06	0.03
V_2O_5	%	0.003	FUS-XRF	0.027	0.045	0.034
LOI	%		FUS-XRF	31.55	25.78	4.84
Total	%	0.01	FUS-XRF	100	100.4	100.5
Sc	ppm	0.1	INAA	8.4	21.3	28.1
V	ppm	5	FUS-ICP	167	259	192
Cr	ppm	5	INAA	306	363	205
Co	ppm	1	FUS-MS	30	55	19
Ni	ppm	20	FUS-MS	230	290	70
Cu	ppm	10	FUS-MS	70	190	20
Zn	ppm	30	FUS-MS	80	120	60
Ag	ppm	0.5	FUS-MS	1.5	4.8	1.9
Sn	ppm	1	FUS-MS	3	3	10
Au	ppb	2	INAA	<2	<2	<2
Y	ppm	2	FUS-ICP	13	31	14
Zr	ppm	4	FUS-ICP	126	452	203
Hf	ppm	0.2	FUS-MS	3.5	10.4	5.5
Nb	ppm	1	FUS-MS	80	123	30
Ta	ppm	0.1	FUS-MS	4.9	8	2.1
W	ppm	1	FUS-MS	3	2	3
Th	ppm	0.1	FUS-MS	8.8	23.2	15.7
U	ppm	0.1	FUS-MS	4.1	10.4	3.2
La	ppm	0.1	FUS-MS	59.1	168	47.8
Ce	ppm	0.1	FUS-MS	101	314	91.3
Pr	ppm	0.05	FUS-MS	11.7	35.6	10.6
Nd	ppm	0.1	FUS-MS	39.3	127	38.4
Sm	ppm	0.1	FUS-MS	6.1	19.8	6.9
Eu	ppm	0.05	FUS-MS	1.57	5.18	1.11
Gd	ppm	0.1	FUS-MS	4.8	16.4	5.3
Tb	ppm	0.1	FUS-MS	0.6	1.8	0.7
Dy	ppm	0.1	FUS-MS	2.9	8	3.2
Ho	ppm	0.1	FUS-MS	0.5	1.2	0.5
Er	ppm	0.1	FUS-MS	1.4	3.1	1.3
Tm	ppm	0.05	FUS-MS	0.18	0.39	0.17
Yb	ppm	0.1	FUS-MS	1.1	2	1
Lu	ppm	0.04	FUS-MS	0.14	0.24	0.14
Be	ppm	1	FUS-ICP	5	6	6
Ga	ppm	1	FUS-MS	7	11	46
Ge	ppm	1	FUS-MS	2	2	4
As	ppm	0.5	INAA	2.9	8.4	28
Rb	ppm	2	FUS-MS	177	300	710
Sr	ppm	2	FUS-ICP	246	344	53
Mo	ppm	2	FUS-MS	5	3	<2
In	ppm	0.2	FUS-MS	<0.2	<0.2	<0.2
Sb	ppm	0.2	INAA	<0.2	<0.2	<0.2
Cs	ppm	0.5	FUS-MS	5.8	9.2	17.9
Ba	ppm	3	FUS-ICP	2114	606	1303
Tl	ppm	0.1	FUS-MS	0.4	0.8	2.4
Pb	ppm	5	FUS-MS	5	11	7
Bi	ppm	0.4	FUS-MS	<0.4	<0.4	<0.4
Br	ppm	0.5	INAA	<0.5	<0.5	<0.5
Ir	ppb	5	INAA	<5	<5	<5
Se	ppm	3	INAA	<3	<3	<3
TREE	ppm			230	703	208
LREE	ppm			217	664	195
La/Yb				54	84	48
Y/Ho				26	26	28
Zr/Hf				36	43	37
Nb/Ta				16	15	14
Zr/Sm				21	23	29
Ti/Eu				120,163	34,819	67,808

adularia-felsitic assemblage, which flows into and cuts the albitite. The typical flow, plumose and radiating textures of the Gifford Creek fenitic rocks surrounding the ironstones, suggest a high degree of undercooling, inferred to be typical of the fine-grained mosaics that constitute the felsitic texture (Shelley, 1993).

4.5. Whole-rock geochemistry

Carbonatites are defined as igneous rocks composed of >50 wt.% igneous carbonate and <20 wt.% SiO_2 (Le Maitre, 2002). Due to unavailability of fresh material, three samples collected for this study are from surface outcrops that show features of intense weathering, and probably secondary fluid alteration processes after/during emplacement (Fig. 5). This limits the insights that can be interpreted from the whole-rock geochemical analyses. Nevertheless these results should be added to the global carbonatite geochemical dataset, and specifically to the ferrocarbonatite available dataset, which is sparse (Chakhmouradian, 2006). Based on immobile elements such as HFSE and REE, when normalized to PM (Primitive Mantle) and MORB (Mid-Ocean Ridge Basalt) as well as their actual concentrations, some interesting geochemical features can be noticed.

A large amount of the original carbonate content had been leached out of samples 205575, 205575B and 205576, during alteration processes. Analytical results are shown in Table 1. Sample 205576 exhibits an increased silica content of up to ~45 wt.% (Table 1). This is interpreted as the result of the intense weathering and relative increase of silica due to leaching of original CaO, Na_2O, MgO and associated volatiles. The fenitic rocks described in this study show bands or laminae of alternating fine-grained aggregates of K-feldspar. This potassic alteration in an open system would explain the K_2O enrichment up to 300 times PM value (Fig. 14A). However, most of the more mobile major oxides, such as Ca, Na and Mg, were leached out due to surface weathering. However, P_2O_5 displays enrichment/redistribution of up to 95 times PM value (Fig. 14A; Table 1; sample 205575B).

The presence of monazite in the samples, suggests that the influence of this mineral on the whole rock geochemistry signature could be significant based on: 1) enrichment of the total REE ranging between 210 and 700 ppm (~6.5 times PM and ~50 times MORB; Fig. 14B); 2) LREE that are more susceptible to enter the monazite crystalline lattice have concentrations from ~200 to ~670 ppm (versus 4 PM and 30 ppm MORB); 3) Th relative to other incompatible trace elements gave between 100 and ~300 times PM average values (Fig. 14B); and 4) high fractionation of LREE and HREE (La/Yb = ~55–85 as referenced to 1.4 PM and 1.2 MORB; Table 1; Fig. 14C).

High field strength element ratios of Zr/Hf, Nb/Ta and Y/Ho are interpreted to be chondritic in basalts, komatiites and peridotites (Rudnick et al., 1993 and references therein), due to their analogous geochemical behaviour (matching ionic radii and charge). The previous Zr/Hf, Nb/Ta and Y/Ho ratios display values that range from 36 to 43, from 14 to 16 and from 26 to 28 respectively (Table 1), whereas PM reference values are ~36, ~17 and ~28 respectively.

Similarly, Zr/Sm ratios are within PM-MORB values (~25). However, the Ti/Eu ratio ranges from ~35,000 to 120,000 whereas Ti/Eu ratio is ~75,000 for PM and MORB average values. No Ce anomaly is noticed, whereas a slight Eu negative anomaly is recorded (Fig. 14C). While ferrocarbonatites average values from Chakhmouradian (2006) show TiO_2, Nb, Ta, Zr and Hf at 0.33 (ranging from 0 to 1.61 wt.%), ~250 (5–~2000), ~9 (0–~40), ~145 (0–~1000) and ~1.5 (0–9) ppm respectively, the Gifford ferrocarbonatite displays averages at ~1.9 (wt.%), ~80, 5, 260, and 6 ppm for the same suite of elements respectively.

Although, HFSE of GFC rocks vary within the ferrocarbonatite range, an enrichment of HFSE is a common but not a distinctive feature in carbonatite rock suites (Chakhmouradian, 2006). The average carbonatite has higher Nb/Ta (35) and Zr/Hf (60) ratios than PM average values (Chakhmouradian, 2006). When comparing the Gifford geochemical data with other ferrocarbonatites such as the Laiwu-Zibo carbonatite in the western Shandong Province, China (Ying et al., 2004), and the Barra do Itapirapua, Brazil (Ruberti et al., 2002), the featuring Nb/Ta and Zr/Hf ratios are comparable (Fig. 14D). Even if the geochemical dataset is limited, and interpretations have to be taken very cautiously, REE–HFSE concentrations and relationships, together with the mineralogy integrated with field observations are

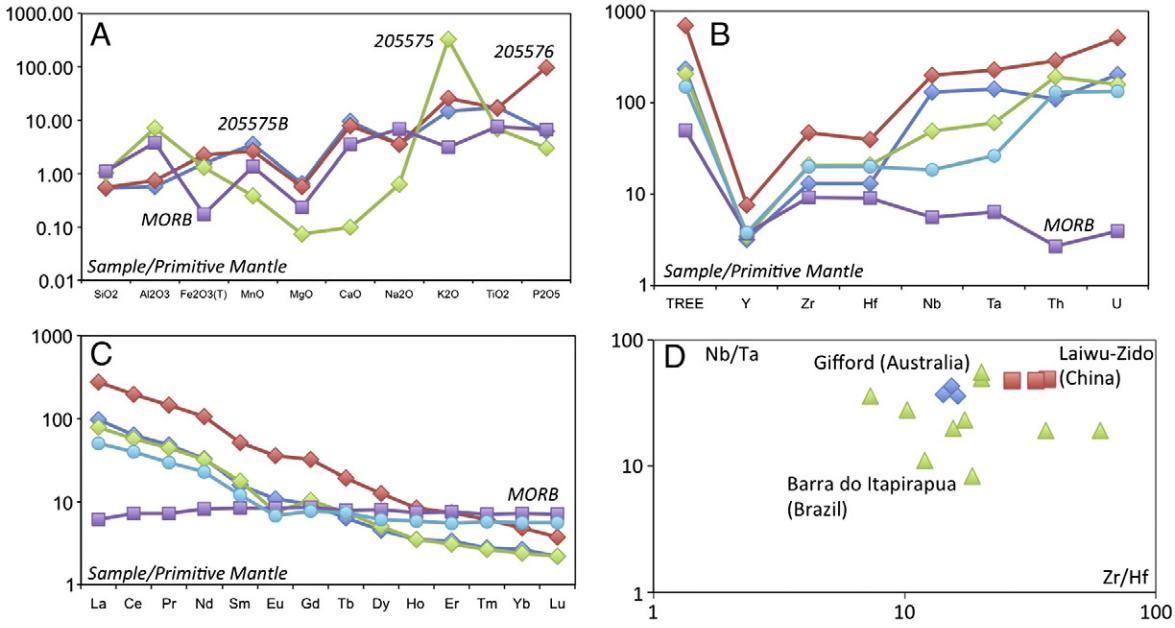

Fig. 14. Whole-rock geochemical plots for samples GSWA 205575, 205575B and 205576 elemental values and major oxides normalized to PM average values from Zindler and Hart (1986). A) Displays major oxide concentrations; B) Presents total REE and HFSE concentrations; C) REE patterns, and D) Nb/Ta versus Zr/Hf ratio (Laiwu–Zido data after Ying et al., 2004; Barra do Itapirapuã data after Ruberti et al., 2002). In (A), (B) and (C) MORB is plotted for comparison. MORB = Mid Ocean Ridge Basalts from Arevalo and McDonough (2010).

supportive of the interpretation of the samples as originated from a ferrocarbonatite suite.

5. Discussion

An understanding of mineralisation associated with alkaline and peralkaline magmatism is based on good evidence that they form through small degrees of partial melting of subcontinental metasomatised mantle lithosphere (Groves et al., 2010 and references therein). Mantle metasomatism was advocated by Bailey (1987), who speculated that rifting may localise mantle degassing (especially C and H) which would metasomatise subcontinental mantle lithosphere and cause partial melting. He pointed out that large quantities of CO_2, F and Cl are emitted from modern rifts such as the East African Rift System. Thus, rifts are the sites of upwelling asthenospheric melts rich in Cl, F, C, P, as well as High Field Strength Elements (Nb–Ta, Zr–Hf, Th). These melts penetrate the lithosphere developing thermal anomalies, metasomatising it and causing further partial melting. The origin of carbonatites, as mentioned in the Introduction, is thought to be linked to low degrees of partial melting in a metasomatised lithospheric mantle and interestingly the carbonated melts have very low viscosities and, based on fluid-flow modelling, these melts can rise to the surface at speeds of up to 65 ms^{-1} (Ernst and Bell, 2010; Genge et al., 1995).

The connection in space and time of some carbonatites with LIPs has led to proposals of a link with mantle plumes, an hypothesis well supported by the Nd, Pb, Sr and noble gases isotope (e.g. $^4He/^3He$ and $^{21}Ne/^{22}Ne$) systematics, which are similar to those of Ocean Island Basalts (OIB) (Bell, 2001). The carbonatite association with LIPs is well demonstrated (Ernst and Bell, 2010) in the Afar and East Africa Rift System (45–0 Ma), the Deccan (65 Ma), Paraná–Etendeka (~133 Ma), the Siberian Traps (~250 Ma), the 380–360 Ma LIP on the eastern margin of the Siberian craton in the vicinity of Yakutsk (e.g. Courtillot and Renne, 2003; Kiselev et al., 2012; Pirajno et al., 2009), the Central Iapetus Magmatic Province (615–550 Ma), the Keeweenawan rift system in North America (1114–1085 Ma) and the Bushveld Igneous Complex (2059–2053 Ma) in South Africa (Ernst and Jowitt, 2013). The time of emplacement of carbonatites in relation to mantle plume activity and the resulting LIP magmatism, may be more varied than previously realised. Bell and Rukhlov (2004) suggested that volatile-rich silicate and carbonated melts form early in the mantle plume-LIP event and flow laterally, intersecting the volatile-rich mantle solidus, where small degrees and small volumes of carbonated partial melts form in a highly metasomatised mantle lithosphere. These melts migrate rapidly upward and are generally confined to the distal and cooler edges of the mantle plume, whereas higher temperature, higher degrees and large melt volumes are confined to the plume head, above which LIPs and mafic–ultramafic intrusions are formed.

Indeed, most carbonatites associated with the major thermal events caused by the upwelling of mantle plumes can be emplaced during pre-, syn- and post-magmatism to within a few million years. For example, the Phalaborwa carbonatite is slightly older (2059 Ma) than the Bushveld mafic–ultramafic units; the Keewenawan carbonatites were emplaced during the main stage of the related magmatism; the carbonatites (and kimberlites) associated with the Siberian Traps were emplaced over a wide area, from the Anabar shield (Maimecha–Kotui province in northern Siberia; Kamo et al., 2003; Pirajno et al., 2009), the Taimyr peninsula to eastern Kazakhstan, with ages ranging from ~234 Ma (post-Siberian Traps) to ~251 Ma (Borisenko et al., 2006). The lateral migration of silicate and carbonate melts is compatible with the fact that the GFC is located about 1400 km from the Warakurna LIP hotspot in the Musgrave Province (Howard et al., 2011) from which lateral flow of plume material may have occurred along the major lithospheric weak zone represented by the WNW-trending Capricorn Orogen and a triple junction between the North Australian Craton, West Australian Craton and the South Australian Craton (Howard et al., 2011; Pirajno and Hoatson, 2012).

It is of interest to point out that carbonatites (and associated alkaline and peralkaline intrusions) are associated with translithospheric breaks and intracontinental strike–slip faults (Bailey, 1993; Ernst and Bell, 2010; Pirajno, 2010). Intracontinental strike–slip zones can reach hundreds of kilometres in length (up to 4000 km in the Transbraziliano strike–slip structure in South America, Ventura Santos et al., 2013) and tens of kilometres in width, commonly marking crustal boundaries and/or terranes and are commonly re-activated time and again during subsequent tectonic and accretionary events. These major structures can be trans-crustal and may reach the sub-continental lithospheric mantle and as such they provide significant channelways for the ascent of magmas and hydrothermal fluids (Pirajno, 2010; Ventura Santos et al., 2013).

The GFC was emplaced along the Lyons River Fault, a major NW-trending structure in the region, which a recent seismic survey across the Gascoyne Province imaged as a deep crustal structure (Johnson et al., 2012) that extends through the Moho into the lithospheric mantle. It follows that other carbonatites could be found along the Lyons River Fault.

The Gifford Creek ferrocarbonatites occur as dyke and sill-like intrusions and are surrounded by or associated with Na–K fenitic aureoles. Fenitic rocks of the GFC are commonly rheomorphic. Fenitisation is dominated by K-feldspar and albite, and varying amounts of aegirine, arfvedsonite, pyrochlore, monazite, bastnaesite and magnetite. In places, K-feldspar and/or albite are dominant and the rock becomes an orthoclasite or an albitite. The predominance of one or the other may be related to depth profiles. According to Le Bas (1987, 1989), potassic fenites (orthoclasite) tend to form around the topmost parts of a carbonatite magmatic system, whereas albitites are from deeply eroded profiles. The carbonatite–ironstone veins and their associated fenitic haloes have a similar mineralogy as those directly associated with the ferrocarbonatite sills and dykes. The apatite and monazite ages, although with error bars showing a substantial overlap and statistically indistinguishable, suggest the possibility of two magmatic phases (Fig. 15), as in fact recorded in the Warakurna Supersuite (Giles Event; 1085–1040 Ma) of the West Musgrave Province, the hotspot centre of the related WLIP (Howard et al., 2011). The first phase at ~1075 Ma was responsible for the emplacement of dykes and sills along the Lyons River fault for which, as mentioned above, seismic profiling indicates that, joining with the sub-parallel Ti Tree Shear Zone, cuts through the crust and reaches into the sub-continental lithospheric mantle (Johnson et al., 2012). Carbonatite melts will have formed in a metasomatised lithospheric mantle, perhaps due to the heat induced by the lateral flow of the Warakurna mantle plume (Pirajno and Hoatson, 2012), resulting in the emplacement of the NW-trending ferrocarbonatite dykes and sills (Fig. 15A). The Lyons River fault system (and the Ti Tree shear zone), was activated time and again during tectonic events in the Gascoyne Province (Cutten et al., in press; Johnson et al., 2012). We suggest that in one of these events, at about 1050 Ma, a small pull-apart structure, possibly defined by the Lyons River Fault and the Bald Hill Lineament, referred to above (Fig. 15), was formed on the sites, where the ferrocarbonatites had been previously intruded at ~1075 Ma. This stimulated the re-activation of the carbonatite system, widening the fenitic halo in the country rocks and producing a sinuous carbonatite veins system which eventually was locally altered to the ironstone veins (Fig. 15B).

Pirajno (2010) discussed the role of mantle plume activity on trans-crustal and trans-lithospheric strike–slip structures in central Asia, where orogen-scale strike–slip faults extend for 100 s to 1000 s of kilometres marking the boundaries of tectonic units and terranes. These strike–slip faults controlled the emplacement of intraplate mafic–ultramafic intrusions, alkaline mafic, felsic and carbonatite magmatism, which coincides with mantle plume(s) activity.

As mentioned above, deep strike–slip faults can act as major conduits for magmas, which in turn induce the formation of magmatic

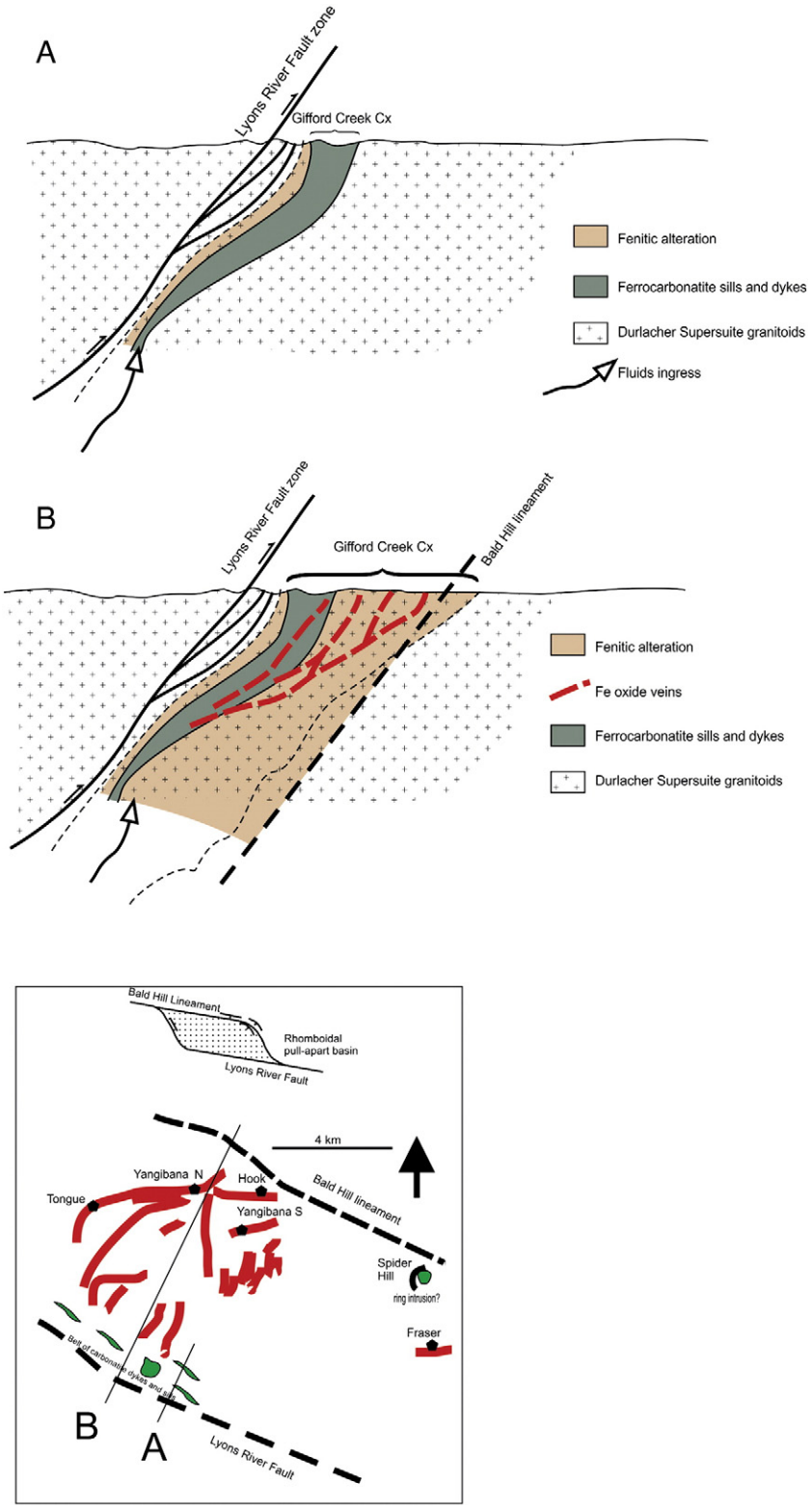

Fig. 15. Two-stage model for the emplacement of ferrocarbonatite sills and dykes at ~1075 Ma along Lyons River Fault (A), followed by strike–slip movements, formation of a pull-apart structure and emplacement of carbonatite-ironstone veins swarm at ~1050 Ma (B); bottom panel shows a schematic spatial distribution of the 1075 Ma ferrocarbonatites dykes and sill and the adjacent 1050 Ma Fe oxide veins swarm emplaced in a pull-apart structure formed during re-activation of the Lyons River Fault; lines A and B in this panel schematically represent the two cross-sections above.

and hydrothermal mineral systems. Furthermore, it is suggested that in the case of mantle plume activity, mantle material could flow laterally from the plume head, towards regions of lower pressure, provided by trans-crustal and/or trans-lithospheric structures and in some cases localised by pull-apart basins formed by strike–slip faults during extensional processes.

Orogen-scale translithospheric strike–slip faults provide the channels for the emplacement of magmas, resulting from lateral flow of

mantle melts along the base of the lithosphere. Lateral flow from mantle plumes head was sustained or facilitated, during stages of extension and movements along the orogen-scale strike–slip faults. Flow of mantle melts into translithospheric strike–slip structures also caused partial melting of a thinned and metasomatised lithosphere, resulting in alkaline magmatic products.

Networks of trans-lithospheric faults, many of which, due to continuing tectonic movements, evolve to strike–slip shear zones, may extend for up to several hundred kilometres long and tens of kilometres wide, characterising many continental regions. This is observed in central and southern Asia, where a giant system of deep strike–slip faults resulted from the closure of the Palaeo- and Neotethys oceans and subsequent accretion processes (Pirajno, 2010 and references therein). These networks of strike–slip shear structures delimit continental deformation zones and lithospheric blocks, which tend to be re-activated time and again during subsequent phases of tectonism and accretion. Seismic, gravity, and magnetotelluric surveys taken across orogenic belts show that deep strike–slip faults commonly extend beyond the Moho, with clear links with the upper mantle (e.g. Pirajno, 2010; Johnson et al., 2012; Vauchez and Tommasi, 2003). Furthermore, we speculate on the possibility of a buried intrusion as a source of the ferrocarbonatite dykes and associated ironstones are exposed. Le Bas (1987) suggested that feldspathic fenites are usually linked to sövite carbonatites and are characterised by albite, co-existing with magnesio-arfvedsonite, aegirine and Fe oxides. Accessory minerals in both carbonatites and fenitic haloes include fluorapatite, magnetite, phlogopite, pyrochlore, quartz, fluorite, barite, bastnaesite and monazite. All of these minerals are observed in the fenitic wallrocks, ferrocarbonatites and ferriferous derivatives of the GFC. Importantly, sövites carry euhedral magnetite (as do most carbonatites; Bailey and Kearns, 2002; Druppel et al., 2005), co-existing with apatite, pyrochlore and micas. Le Bas (1987) also emphasised that the ankeritic ferrocarbonatites, which evolve by magmatic differentiation from sövites, tend to be of the greatest interest for economic rare metal mineralization potential. Once the carbonatite magma has crystallised, its residue is rich in volatiles (e.g. CO_2), thereby becoming a volatile-rich fluid. This would be followed by progressive alteration of the primary minerals, forming calcite and the dissolution of Fe-bearing minerals. This leads to replacement of the existing mineral phases, beginning along microfractures and gradually extending to form veinlets, which then coalesce into larger veins. In this somewhat simplified evolutionary scheme, it must be emphasised that fenitisation and iron-dominant alteration would commonly be a complex and multiphase process. Chemical reactions associated with fenitisation and Fe oxide alteration, in the case of the GFC, can totally obscure the original rock type(s).

In the GFC, mineralisation is mostly hosted in the fenitic haloes and as far as is presently known consists of REE, U, Th, Nb and Fe. Furthermore, we suggest that the GFC was likely the result of alkaline-carbonatite magmatism derived from partial melting of a metasomatised sub-continental mantle lithosphere associated with the lateral flow of the mantle plume, which is thought to be linked with the ~1075 Ma Warakurna LIP. If our hypothesis is correct the GFC is first to be recognised in the Warakurna LIP, thereby opening the door to more discoveries of carbonatites and associated alkaline complexes.

6. Concluding remarks

The sills and dykes of the GFC, are surrounded by zones of fenitisation (albite and K-feldspar mainly) due to wallrock interactions and laterally extending for tens of metres. The fenites commonly exhibit extensive fluidisation textures due to the exsolution of abundant volatiles. The fluidised material was emplaced as arcuate and sinuous veins, which in later paragenetic stages were progressively replaced by hydrothermal Fe oxides. Previous studies coupled with field and petrographic observations suggest that a sövite plutonic complex may underlie and may be the source of the ferrocarbonatites.

To summarise, in this contribution we report:

1) Field, petrographic, XRD, SEM, EPMA, and whole rock major and trace element geochemistry (XRF and ICP-MS) of ferrocarbonatite samples.

2) We provide a genetic model for the ironstone veins that are associated with the ferrocarbonatites and accompanying fenitic alteration haloes.

3) In-situ U–Pb dating of apatite grains by LA-ICP-MS from a sample of ferrocarbonatite, yielding an average age of 1075 ± 35 Ma (MSWD = 2.2), while monazite grains from fenitic rocks associated with the ironstone veins returned a concordia age of 1050 ± 24 Ma.

4) The apatite age is close to the age of the Warakurna LIP, which has its "hot spot" in the Musgrave Province in central Australia. The monazite age likely records a second event associated with strike–slip movements along the Lyons River Fault.

5) Based on the world-wide occurrences of carbonatite in LIPs (Ernst and Bell, 2010; Ernst and Jowitt, 2013), our age data would confirm that other carbonatites may well be present within the Warakurna LIP. This we consider a significant finding, due to the increasing importance of REE mineral systems related to carbonatites.

Acknowledgements

Mr Richard Clarke carried out EDX and XRPD analyses at the Chem Centre (Curtin University of Technology, Perth, Western Australia). We thank Marcus Sweetapple and Monica A. Kusiak, who gave insightful and detailed reviews of an earlier version of this paper. Richard Ernst and an anonymous reviewer also gave insightful comments, which considerably improved our paper. Franco Pirajno published with permission of the Executive Director of the Geological Survey of Western Australia.

Appendix II. Supplementary data

Supplementary data to this article can be found online at http://dx.doi.org/10.1016/j.lithos.2014.05.012.

Appendix I

In-situ U–Pb dating results for apatite by LA-ICP-MS.

Sample	Analyses	$^{238}U/^{206}Pb$	2s error	$^{207}Pb/^{206}Pb$	2s error	$^{208}Pb/^{232}Th$	2s error	$^{208}Pb/^{206}Pb$	2s error	F206	Rad.$^{206}Pb/^{238}U$	Rad.$^{206}Pb/^{238}U$ age (Ma)	2s error
205577	Ap1	1.4890	0.0500	0.6761	0.0110	1.0759	0.0229	1.6213	0.0203	0.73	0.1814	1075	36
	Ap2	1.4585	0.0510	0.6802	0.0112	1.0252	0.0663	1.6382	0.0265	0.73	0.1818	1077	38
	Ap6	0.6829	0.0456	0.7955	0.0153	2.5569	0.3413	1.8904	0.0294	0.87	0.1831	1084	72
	Ap7	0.5140	0.0224	0.8234	0.0092	1.1846	0.0128	2.0114	0.0178	0.91	0.1775	1053	46
	Ap8	0.3335	0.0107	0.8464	0.0090	0.9739	0.0102	2.0826	0.0093	0.94	0.1897	1120	36
	Ap9	0.4820	0.0476	0.8292	0.0178	5.0895	0.3341	1.9396	0.0449	0.92	0.1747	1038	103
	Ap10	0.5550	0.0281	0.8206	0.0149	3.9255	0.1755	1.9216	0.0302	0.91	0.1705	1015	51

Appendix III

EPMA analysis on columbite grains.

Sample/Element (wt.%)	Ta	W	Mg	Sc	Sn	U	Fe	Mn	Yi	Nb	Zr	Y	O	Total
197988	0.09	0.12	0.09	0.00	0.00	0.00	16.76	0.52	2.07	50.64	0.01	0.06	28.27	98.64
197989	0.09	0.18	0.10	0.01	0.00	0.00	16.04	0.62	2.40	50.59	0.09	0.06	28.35	98.55
197987	0.26	0.12	0.07	0.01	0.00	0.02	15.89	0.69	1.00	52.31	0.00	0.07	28.10	98.53
197991	0.13	0.11	0.09	0.00	0.00	0.00	16.40	0.58	1.42	51.46	0.02	0.06	28.11	98.38
197993	0.02	0.08	0.10	0.00	0.00	0.01	16.18	0.59	1.48	51.61	0.00	0.06	28.13	98.26
197990	0.25	0.17	0.13	0.01	0.02	0.00	15.92	0.67	1.51	51.25	0.14	0.07	28.09	98.24
197992	0.02	0.05	0.11	0.01	0.00	0.01	16.11	0.60	1.25	51.81	0.00	0.05	28.04	98.07

EPMA analysis on amphibole grains.

SAMPLE/element (wt.%)	Na	F	S	Cr	K	Mg	Al	Cl	M	Ca	Si	P	Ba	Fe	Ti	O	Total
198000	9.31	0.00	0.01	0.08	0.06	0.52	0.11	0.00	0.00	0.52	25.22	0.00	0.00	21.23	2.10	40.16	99.31
197998	9.01	0.00	0.00	0.06	0.03	0.80	0.14	0.00	0.09	0.79	25.40	0.00	0.00	19.59	2.45	40.36	98.74
197999	8.83	0.00	0.00	0.11	0.04	0.62	0.07	0.00	0.04	0.85	25.23	0.00	0.00	19.80	2.85	40.28	98.72
197997	8.70	0.00	0.00	0.07	0.08	1.07	0.13	0.01	0.06	0.95	25.43	0.00	0.00	19.53	2.23	40.35	98.61
197996	9.52	0.00	0.00	0.07	0.03	0.67	0.03	0.01	0.00	0.02	25.42	0.00	0.00	20.12	2.42	40.18	98.52
198001	9.16	0.00	0.00	0.05	0.04	0.86	0.05	0.00	0.00	0.10	25.55	0.00	0.00	18.12	3.72	40.66	98.33
198004	8.85	0.00	0.01	0.12	0.00	0.72	0.04	0.00	0.01	0.64	25.34	0.00	0.L00	20.24	2.19	40.05	98.20
197997	4.44	1.52	0.00	0.08	3.51	7.99	0.19	0.00	0.00	1.31	26.54	0.00	0.00	11.29	0.56	42.11	99.56
197996	5.52	0.94	0.00	0.01	2.17	6.55	0.23	0.00	0.02	0.28	26.56	0.00	0.00	14.39	0.54	41.75	98.96
197998	4.46	0.73	0.00	0.03	1.56	5.91	0.73	0.02	0.10	0.43	26.61	0.00	0.00	15.84	0.39	41.75	98.54
198002	5.18	0.62	0.00	0.01	0.72	7.07	0.12	0.00	0.00	0.30	26.91	0.00	0.00	15.42	0.09	41.98	98.43
198003	5.44	0.67	0.00	0.16	0.71	7.72	0.16	0.00	0.03	0.26	26.64	0.00	0.00	14.13	0.19	41.98	98.10
197996	4.82	0.32	0.00	0.03	0.35	6.23	0.41	0.01	0.05	0.24	25.96	0.00	0.00	18.31	0.12	41.24	98.09

References

Ackerman, L., Jelínek, E., Medaris, G., Ježek Wolfgang, S., Strnad, L., 2009. Geochemistry of Fe-rich peridotites and associated pyroxenites from Horní Bory, Bohemian Massif: insights into subduction-related melt–rock reactions. Chemical Geology 259, 152–167.

Andersen, T., 1984. Secondary processes in carbonatites: petrology of "rødberg" (hematite–calcite–dolomite carbonatite) in the Fen Central Complex, Telemark (South Norway). Lithos 17, 227–245.

Arevalo, R., McDonough, R.F., 2010. Chemical variations and regional diversity observed in MORB. Chemical Geology 271, 70–85.

Bailey, D.K., 1987. Mantle metasomatism — perspective and prospect. Geological Society, London, Special Publication 30, 1–14.

Bailey, D.K., 1993. Carbonate magmas. Journal of the Geological Society, London 150, 637–651.

Bailey, D.K., Kearns, S., 2002. High-Ti magnetite in some fine-grained carbonatites and the magmatic implications. Mineralogical Magazine 66 (3), 379–384.

Begg, G.C., Griffin, W.L., Napatov, L.M., O'Reilly, S.Y., Grand, S.P., O'Neill, C.J., Hronsky, J.M.A., Poudjom Djomani, Y., Swain, C.J., Deen, T., Bowden, P., 2009. The lithospheric architecture of Africa: seismic tomography, mantle petrology and tectonic evolution. Geosphere 5, 23–50.

Begg, G.C., Hronsky, J.A.M., Arndt, N.T., Griffin, W.L., O'Reilly, S.Y., Hayward, N., 2010. Lithospheric, cratonic and geodynamic setting of Ni–Cu–PGE sulfide deposits. Economic Geology 105, 1057–1070.

Bell, K., 2001. Carbonatites: relationships to mantle-plume activity. In: Ernst, R.E., Buchan, K.L. (Eds.), Mantle Plumes: Their Identification through Time. Geological Society of America Special Paper, 352, pp. 267–290.

Bell, K., Kjarsgaard, B.A., Simonetti, A., 1999. Carbonatites—into the twenty-first century. Journal of Petrology 39, 1839–1845.

Bell, G.C., Rukhlov, A.S., 2004. Carbonatite from the Kola Alkaline Province: origin, evolution and source characteristics. In: Wall, F., Zaitsev, A.N. (Eds.), Phoscorites and Carbonatites from Mantle to Mine: the Key Example of the Kola Alkaline Province. Mineralogical Society, London, 10, pp. 421–455.

Borisenko, A.S., Sotnikov, V.I., Izokh, A.E., Polyakov, G.V., Obolensky, A.A., 2006. Permo-Triassic mineralization in Asia and its relation to plume magmatism. Russian Geology and Geophysics 47, 166–182.

Chakhmouradian, A.N., 2006. High-field-strength elements in carbonatitic rocks: geochemistry, crystal chemistry and significance for constraining the sources of carbonatites. Chemical Geology 235, 138–160.

Chakhmouradian, A.R., Wall, F., 2012. Rare earth elements: minerals, mines, magnets (and more). Elements 8, 333–340.

Chen, W., Simonetti, A., 2013. In-situ determination of major and trace elements in calcite and apatite, and U–Pb ages of apatite from the Oka Carbonatite Complex: insights into a complex crystallization history. Chemical Geology 335, 151–172.

Chew, D.M., Sylvester, P.J., Tubrett, M.N., 2011. U–Pb and Th–Pb dating of apatite by LA-ICP-MS. Chemical Geology 280, 200–216.

Courtillot, V.E., Renne, P.R., 2003. On the ages of flood basalt events. Geoscience 335, 113–140.

Cox, R.A., Wilton, D.H.C., 2006. U–Pb Dating of Perovskite by LA-ICP-MS: An Example.

Cutten, H., Johnson, S.P., Thorne, A.M., Pirajno, F., Wingate, M.T.D., Zwingmann, H., Blay, O., 2014. Structure, Deformation and Mineral Systems of the Edmund and Collier Basins, Capricorn Orogen. Geological Survey of Western Australia, Report 127, (in press).

D'Orazio, M., Innocenti, F., Tonarini, S., Doglioni, C., 2007. Carbonatites in a subduction system: the Pleistocene alvikites from Mt Vulture (southern Italy). Lithos 98, 313–334.

Downes, H., Wall, F., Demény, A., Szabó, Cs., 2012. Continuing the carbonatite controversy. Mineralogical Magazine 76, 255–257.

Druppel, K., Hoefs, J., Okrusch, M., 2005. Fenitizing processes induced by ferrocarbonatite magmatism at Swartbooisdrift, NW Namibia. Journal of Petrology 46, 377–406.

Ebinger, C.J., Sleep, N.H., 1998. Cenozoic magmatism throughout east Africa resulting from the impact of a single plume. Nature 395, 788–791.

Eggler, D.H., 1989. Carbonatites, primary melts, and mantle dynamics. In: Bell, K. (Ed.), Carbonatites: Genesis and Evolution. Unwin Hyman, London, pp. 561–579.

Ernst, R.E., Bell, K., 2010. Large Igneous Provinces (LIPs) and carbonatites. Mineralogy and Petrology 98, 55–76.

Ernst, R.E., Jowitt, S.M., 2013. Large Igneous Provinces (LIPs) and metallogeny. Economic Geology Special Publication 17, 17–51.

Flint, D., Abeysinghe, P.B., 2000. Geology and mineral resources of the Gascoyne Region. Geological Survey of Western Australia, Record 2000/7.

Freestone, I.C., Hamilton, D.L., 1980. The role of liquid immiscibility in the genesis of carbonatites — an experimental study. Contributions Mineralogy and Petrology 73, 105–117.

Gellatly, D. C., 1975. Yangibana Creek U–Th–RE-base metal prospect, Gascoyne Goldfield, WA, Final Report Amax Exploration (Australia) Inc. (unpublished).

Genge, M.J., Price, G.D., Jones, A.P., 1995. Molecular dynamics simulation of $CaCO_3$ melts to mantle pressures and temperatures: implications for carbonatite magmas. Earth and Planetary Science Letters 131, 225–238.

Gittins, J., 1989. The origin and evolution of carbonatite magmas. In: Bell, K. (Ed.), Carbonatites. Genesis and Evolution Unwin Hyman Ltd., London, pp. 580–600.

Gittins, J., Harmer, R.E., 1997. What is ferrocarbonatite? A revised classification. Journal of African Earth Sciences 25, 159–168.

Groves, D.I., Bierlein, F.P., Meinert, L.D., Hitzman, L.W., 2010. Iron Oxide Copper–Gold (IOCG) deposits through Earth history: implications for origin, lithospheric setting, and distinction from other epigenetic iron oxide deposits. Economic Geology 105, 641–654.

Hastings Rare Metals Ltd., 2012. Australian Stock Exchange (ASX) Announcement, 29th March 2012 (unpublished); http://www.hastingsraremetals.com/projects/yangibana-project/previous-exploration/.

Hoatson, D.M., Jaireth, S., Miezitis, Y., Hoatson, D.M., Jaireth, S., Miezitis, Y., 2011. The Major Rare-Earth-Element Deposits of Australia: Geological Setting, Exploration and Resources. Geoscience Australia Report, (204 pp.).

Howard, H.M., Smithies, R.H., Evins, P.M., Kirkland, C.L., Werner, M., Wingate, M.T.D., Pirajno, F., 2011. Explanatory Notes for the West Musgrave Province. Geological Survey of Western Australia, Record 2011/4, (349 pp.).

Johnson, S.P., Sheppard, S., Rasmussen, B., Muhling, J.R., Fletcher, I.R., Wingate, M.T.D., Kirkland, C.L., Pirajno, F., 2009. Meso- to Neoproterozoic Reworking in the Gascoyne Complex and What It Means for Mineral Exploration. Geological Survey of Western Australia, Record 2009/2.

Johnson, S.P., Sheppard, S., Wingate, M.T.D., Kirkland, C.L., Belousova, E.A., 2011a. Temporal and Hafnium Isotopic Evolution of the Glenburgh Terrane Basement: An Exotic Crustal Fragment in the Capricorn Orogen. Geological Survey of Western Australia, Report 110, (27 pp.).
Johnson, S.P., Sheppard, S., Rasmussen, B., Wingate, M.T.D., Kirkland, C.L., Muhling, J.R., Fletcher, I.R., Belousova, E.A., 2011b. Two collisions, two sutures: punctuated pre-1950 Ma assembly of the West Australian Craton during the Ophthalmian and Glenburgh Orogenies. Precambrian Research 3–4, 239–262.
Johnson, S.P., Sheppard, S., Thorne, A.M., Rasmussen, B., Fletcher, I.R., Wingate, M.T.D., Cutten, H.N., 2011c. The role of the 1280–1250 Ma Mutherbukin Tectonic Event in shaping the crustal architecture and mineralization history of the Capricorn Orogen, in GSWA 2011 extended abstracts: promoting the prospectivity of Western Australia. Geological Survey of Western Australia, Record 2011/2, pp. 1–3.
Johnson, S.P., Thorne, A.M., Cutten, H.N., Blay, O.A., 2012. Geological Interpretation of the Western Capricorn Orogen in Capricorn Orogen Seismic and Magnetotelluric (MT) Workshop 2011. Geological Survey of Western Australia, Record 2011/25.
Kamo, S., Czamanske, G., Amelin, Y., Fedorenko, V.A., Davis, D.W., Trofimov, V.R., 2003. Rapid eruption of Siberian flood-volcanic rocks and evidence for coincidence with the Permian–Triassic boundary and mass extinction at 251 Ma. Earth and Planetary Science Letters 214, 75–91.
Kiselev, A.I., Ernst, R.E., Yarmoluk, V.V., Egorov, K.N., 2012. Radiating rifts and dyke swarms of the middle Paleozoic Yakutsk plume of eastern Siberian craton. Journal of Asian Earth Sciences 45, 1–16.
Kjarsgaard, B.A., Hamilton, D.L., 1989. The genesis of carbonatites by immiscibility. In: Bell, K. (Ed.), Carbonatites: Genesis and Evolution. Unwin Hyman, London, pp. 388–404.
Kjarsgaard, B.A., Peterson, T., 1991. Nephelinite–carbonatite liquid immiscibility at Shombole volcano, East Africa: petrographic and experimental evidence. Mineralogy and Petrology 43, 293–314.
Le Bas, M.J., 1987. Nephelinites and carbonatites. In: Fitton, J.G., Upton, B.G.J. (Eds.), Alkaline Igneous Rocks. Geological Society Special Publication, 30, pp. 53–86.
Le Bas, M.J., 1989. Diversification of carbonatites. In: Bell, K. (Ed.), Carbonatites — Genesis and Evolution. Unwin Hyman, London, pp. 70–88.
Le Maitre, R.W., 2002. Igneous Rocks; a Classification and Glossary of Terms. Cambridge University Press, Cambridge, USA, (236 pp.).
Lentz, D.R., 1999. Carbonatite genesis: a reexamination of the role of intrusion-related pneumatolytic skarn processes in limestone melting. Geology 27 (4), 335–338.
Ludwig, K.R., 2003. User's Manual for IsoPlot 3.00: A Geochronological Toolkit for Microsoft Excel.
Martin, D.McB., Sheppard, S., Thorne, A.M., Farrell, T.R., Groenewald, P.B., 2006. Proterozoic Geology of the Western Capricorn Orogen — A Field Guide. Geological Survey of Western Australia, Record 2006/18, p. 41.
Mathias, M., 1956. The petrology of the Messum igneous complex. South-West Africa: Transaction of the Geological Society of South Africa 59, 23–57.
Mitchell, R.H., 2005. Carbonatites and carbonatites and carbonatites. The Canadian Mineralogist 43, 2049–2068.
Mutschler, F.E., Griffin, M.E., Scott Stevens, D., Shannon, S.S., 1985. Precious metal deposits related to alkaline rocks in the North American Cordillera — an interpretive view. Transaction of the Geological Society of South Africa 88, 355–377.
Newcrest Mining Ltd., 1991. Gifford Creek report for the period 1/1/91 to 31/12/91. Department of Mines and Petroleum, open file report A35093, vol. I (unpublished).
Pearson, J.M., 1996. Alkaline rocks of the Gifford Creek Complex, Gascoyne Province, Western Australia: their petrogenetic and tectonic significance. PhD thesis (unpublished), University of Western Australia, Department of Geology and Geophysics, 286 pp.
Pearson, J.M., Taylor, W.R., 1996. Mineralogy and geochemistry of fenitized alkaline ultrabasic sills of the Gifford Creek Complex, Gascoyne Province, Western Australia. The Canadian Mineralogist 34, 201–219.
Pearson, J.M., Taylor, W.R., Barley, M.E., 1996. Geology of the alkaline Gifford Creek Complex, Gascoyne Complex, Western Australia. Australian Journal of Earth Sciences 43, 299–309.
Pirajno, F., 2000. Ore Deposits and Mantle Plumes. Kluwer Academic Publishers, Dordrecht, (556 pp.).
Pirajno, F., 2010. Intracontinental strike–slip faults, associated magmatism, mineral systems and mantle dynamics; examples from NW China and Altay-Sayan (Siberia). Journal of Geodynamics 50, 325–346.
Pirajno, F., 2012. Effects of metasomatism on mineral systems and their host rocks: alkali metasomatism, skarns, greisens, tourmalinites, rodingites, black-wall alteration and listvenites. In: Harlov, D.E., Austrheim, H. (Eds.), Metasomatism and Metamorphism: the Role of Fluids in Crustal and Upper Mantle Processes. Lecture Series in Earth Science. Springer, pp. 203–252.
Pirajno, F., González-Álvarez, I., 2013. The Ironstone Veins of the Gifford Creek Ferrocarbonatite Complex, Gascoyne Province. Geological Survey of Western Australia Record 2013/12.
Pirajno, F., Hoatson, D.M., 2012. A review of Australia's Large Igneous Provinces and associated mineral systems: implications for mantle dynamics through geological time. Ore Geology Reviews 48, 2–54.
Pirajno, F., Ernst, R.E., Borisenko, A.S., Fedoseev, G., Naumov, E.A., 2009. Intraplate magmatism in Central Asia and China and associated metallogeny. Ore Geology Reviews 35, 114–136.
Pirajno, F., Sheppard, S., Johnson, S., González-Álvarez, I., Thorne, A., Cutten, H., 2010. The Gifford Creek Carbonatite Complex and associated REE, U and Fe oxides mineralisation, Gascoyne Province, Western Australia. Abstracts Volume IAGOD Symposium, Adelaide 2010, pp. 115–116.
Pooley, G.D., 1989. Annual Report, Reconnaissance drilling programme — indicated rare earth element potential, Gascoyne Mineral Field, Western Australia. E09/95 Annual Report. Hurlstone Pty Ltd, unpublished, lodged to Department of Mines and Petroleum, Accession No. 25937, M 5479.
Ruberti, E., Castirina, F., Censi, P., Comin-Chiaramonti, P., Gomes, C.B., Antonini, P., Andrade, F.R.D., 2002. The geochemistry of the Barra do Itapirapuã carbonatite (Ponta Grossa Arch, Brazil): a multiple stockwork. Journal of South American Earth Sciences 15, 215–228.
Rudnick, R.L., Gao, W.F., Chappell, B.W., 1993. Carbonatite metasomatism in the northern Tanzania mantle: petrographic and geochemical characteristics. Earth and Planetary Science Letters 114, 463–475.
Shelley, D., 1993. Igneous and Metamorphic Rocks under the Microscope; Classification, Textures, Microstructures and Mineral Orientations. Chapman & Hall, London, (445 pp.).
Sheppard, S., Rasmussen, B., Muhling, J.R., Farrell, T.R., Fletcher, I.R., 2007. Grenvillian-aged orogenesis in the Paleoproterozoic Gascoyne Complex, Western Australia: 1030–950 Ma reworking of the Proterozoic Capricorn orogeny. Journal of Metamorphic Geology 25, 477–494.
Sheppard, S., Johnson, S.P., Wingate, M.T.D., Kirkland, C.L., Pirajno, F., 2010. Explanatory notes for the Gascoyne Province. Geological Survey of Western Australia, (336 pp.).
Sheppard, S., Bodorkos, S., Johnson, S.P., Wingate, M.T.D., Cl, Kirkland, 2011. The Paleoproterozoic Capricorn Orogeny: intracontinental reworking not continent–continent collision. Geological Survey of Western Australia, Report 108, (33 pp.).
Simonetti, A., Neal, C.R., 2010. In-situ chemical, U–Pb dating, and Hf isotope investigation of megacrystic zircons, Malaita (Solomon Islands): evidence for multi-stage alkaline magmatic activity beneath the Ontong Java Plateau. Earth and Planetary Science Letters 295, 251–261.
Solovova, I.P., Girnis, A.V., Kogarko, L.N., Kononkova, N.N., Stoppa, F., Rosatelli, G., 2005. Composition of magmas and carbonate-liquid immiscibility in the Vulture alkaline igneous complex, Italy. Lithos 85, 113–128.
Stoppa, F., Rosatelli, G., Wall, F., Jeffries, T., 2005. Geochemistry of carbonatite–silicate pairs in nature: a case history from central Italy. Lithos 85, 26–47.
Taylor, G., Eggleton, R.A., 2001. Regolith Geology and Geomorphology. Wiley & Sons, Ltd., Chichester, (375 pp.).
Tera, F., Wasserburg, G.J., 1972. U–Th–Pb systematics in the Apollo 14 basalts an the problem of initial Pb in lunar rocks. Earth and Planetary Science Letters 14, 281–304.
Thomson, S.N., Gehrels, G.E., Cecil, R., Ruiz, J., 2009. Exploring Routine Laser Ablation Multicollector ICP-MS U–Pb Dating of Apatite. AGU Fall Meeting.
Vauchez, A., Tommasi, A., 2003. Wrench faults down to the asthenosphere: geological and geophysical evidence and thermo-mechanical effects. The Geological Society, London, Special Publication 210, 15–34.
Ventura Santos, R., Gouveia de Oliveira, C., Vaz Parente, C., da Glória Motta Garcia, M., Dantas, E.L., 2013. Hydrothermal alteration related to a deep mantle source controlled by a Cambrian intracontinental strike–slip fault: evidence for the Meruoca felsic intrusion associated with the Transbraziliano Lineament, Northeastern Brazil. Journal of South American Earth Sciences 43, 33–41.
Watkinson, D.H., Wyllie, P.J., 1971. Experimental study of the join $NaAlSiO_4$–$CaCO_3$–H_2O and the genesis of alkali rock–carbonatite complexes. Journal of Petrology 12, 357–378.
Whitney, D.L., Evans, B.W., 2010. Abbreviations for names of rock-forming minerals. American Mineralogits 95, 185–187.
Wingate, M.T.D., Giddings, J.W., 2000. Age and palaeomagnetism of the Mundine Well dyke swarm, Western Australia: implications for an Australia–Laurentia connection at 755 Ma. Precambrian Research 100, 335–357.
Wingate, M.T.D., Pirajno, F., Morris, P.A., 2004. Warakurna large igneous province: a new Mesoproterozoic large igneous province in west-central Australia. Geology 32, 105–108.
Woolley, A.R., Kjarsgaard, B.A., 2008. Carbonatites Occurrences of the World: Map and Database. Geological Survey of Canada, Open File 5796.
J.Ying, J., X.Zhou, X., H.Zhang, H., 2004. Geochemical and isotopic investigation of the Laiwu-Zibo carbonatites from western Shandong Province, China, and implications for their petrogenesis and enriched mantle sourceLithos 75, 413–426.
Zindler, A., Hart, S., 1986. Chemical geodynamics. Annual Review of Earth and Planetary Sciences 14, 493–571.